Electromechanical behaviour of piezoelectric actuators with partially debonded adhesive layers

by

Huan Hu

A thesis submitted in partial fulfillment of the requirements for the degree of

Master of Science

Department of Mechanical Engineering
University of Alberta

Abstract

The electromechanical behaviour of piezoelectric actuators and the adhesive layer, which connects the actuator and the host structure can have an effect on the performance of smart piezoelectric structures. In this study, a newly thin-sheet piezoelectric actuator model with an adhesive layer, which undergoes bending deformation, is proposed. This thesis is to present a comprehensive theoretical study of the effects of material mismatch and geometry parameters of the piezoelectric actuator model upon the coupled electromechanical characteristics of piezoelectric actuator systems. The emphasis of the current study is on the load transfer, local stress field, axial force and bending moment near the imperfectly bonded actuators. Theoretical electromechanical solutions to the interfacial stresses based on the integral governing equations are provided using Chebyshev polynomial expansion. Detailed numerical simulations are conducted to evaluate the effects of the geometry and the material mismatch of the piezoelectric actuator and adhesive layer upon the actuating process. The effects of the interfacial debonding are also presented and discussed. The results indicate that the geometry and material properties of the actuator system affect the stress distribution, load transfer, axial force and bending moment significantly, and the corresponding effects have been discussed and analyzed in detail. This study could provide some new insights into the design of piezoelectric actuator system.

Acknowledgements

This work has been made possible with the support of many people. My first note of gratitude goes to my supervisor, Prof. Xiaodong Wang, whose precious guidance and encouragement, were indispensable in the completion of this thesis. He taught me not only undertaking research but also enhancing my vision and independent thinking ability. This experience has been, and will continue to be, invaluable to me. I would also like to thank all of my master committee members Dr. Zengtao Chen, Dr. Zhigang Tian and Dr. Peter Schiavone. I appreciate their valuable suggestions and advice on my work and thank them for reviewing my dissertation.

I am very thankful to all of my colleagues in our ASML Lab, Dr. Huangchao Yu, Dr. Mohamad Molavi Nojumi and Chen Wang. It has been an extremely enjoyable experience working with them. I got their help, support and obtained valuable friendship during my master study.

I could not have come so far without the support of my family. I would like to mention my parents, Tingfang Hu and Xianhua Ou, for their endless love. Because of their support, I could have the chance to pursue my dream. It would have been difficult to get to where I am without their encouragement and support. Finally, I thank my husband, Zhengwei Li, the one who pushes me to take one more step when I feel I have reached the end. Thank him for always being there for me. My special thanks to my cutest children, Jennifer Li and Daniel Li. They bring me so much enjoy and make me better understand responsibility.

Table of Contents

List of Tables

List of Figures

Chapter 1: Introduction and objectives

This chapter is divided into three sections. The background and motivation of the thesis topics are presented in Section 1.1. The research objectives are provided in Section 1.2. Section 1.3 lists outline of the thesis.

1.1 Background and motivation

In a common definition, smart materials differ from the ordinary materials since they can change properties in a predictable or controllable manner in response to external stimuli (Newnham and Ruschau, 1993). For linear systems the materials could return to their original states once the external stimulus expires and all changes are reversible. The stimuli could be temperature, forces, electric or magnetic fields, chemical compounds, and humidity. There is a wide range of different smart materials, which include shape-memory alloys, piezoelectric materials, magnetostrictive materials, electroactive polymers and bicomponent fibers (Otsuka and Wayman, 1999). Over the past several decades, the smart materials and systems have experienced tremendous growth through research and engineering. They also have been harnessed in a variety of high-tech and everyday applications, which range from sensors/actuators or pediatric cardiovascular devices to electroactive polymers (Levi et al., 2008; Schwartz, 2009). Piezoelectric materials are very popular as a kind of smart material and they have been widely used in practical applications for the ability to transform electrical energy to mechanical energy and vice versa, functioning as both actuators and sensors (Tani et al., 1998).

Piezoelectric actuators/sensors have been applied to the control of static and dynamic deformation of structures, vibration, noise and wave propagation (Boller, 2000; Duan et al., 2010; Na and Baek, 2018a). Usually, piezoelectric actuator/sensor is surface-bonded onto or embedded into a structure in the form of thin-sheets. In order to optimize the effectiveness and reliability of the piezoelectric actuators/sensors systems, the actuating/sensing process and the resulting electromechanical response should be well understood. The electromechanical behaviour of the piezoelectric actuator system is the first issue that needs to be evaluated. The second concern lies in the bonding condition of the interface between the actuator and host, particularly the adhesive layer and the interfacial debonding. The local stress field near the interface is very important since it can affect the property of the actuator and the bonding condition. Interfacial debonding condition may occur when high local electromechanical stress field is generated or poor bonding condition around the edges of the actuators/sensors (Denoyer and Kwak, 1996; Park et al., 2000b; Rabinovitch and Vinson, 2002a; Tylikowski, 2001a).

To address above issues, various works have been carried out to uncover the electromechanical behaviour of piezoelectric actuator systems by considering different geometries and materials, as well as load combinations. The pioneer study was made by Crawley et al.(Crawley and Anderson, 1990; Crawley and De Luis, 1987). An analytical model was presented by treating axial stress across the thickness of piezoelectric actuator as uniform or linear. Luo and Tong (Luo and Tong, 2002a,b) developed a theoretical model including adhesive layers for a PZT smart beam, and analyzed the effects of debonding on the distributions of strain, stress and displacement. Plate and shell models have also been ex-

tensively used in the study of electromechanical behaviour of smart piezoelectric structures (Reddy, 1999; Tzou and Gadre, 1989; Zhang et al., 2019). Considering the disadvantages of predicting the interfacial stress field near the ends of piezoelectric actuators in all works mentioned above by modeling the piezoelectric layers as beams, plates and shells. Wang et al. (Wang and Meguid, 2000) first examined the coupled electromechanical behaviour of a thin piezoceramic actuator embedded in or bonded to an infinite elastic medium under inplane mechanical and electrical loadings. Here, the host structure is treated as a semi-infinite plane because both length and thickness of the piezoelectric actuator are much smaller than the size of the host. The actuator is modelled as an electro-elastic line and only the interfacial shear stress is considered. The results showed that this treatment is an effective way to analyze local stress and load transfer between the actuator and the host structure. Jin et al. (Jin and Wang, 2011a,b) modified the model presented by Wang (Wang and Meguid, 2000) by adding a bonding layer between the piezoelectric actuator and the host structure. Yu et al. (Yu and Wang, 2016) further modified the electro-elastic line model by introducing bending deformation of the actuator. However, in the model, the adhesive layer is not considered and thus the model is only suitable for very rigid adhesive layers. An analytical model to study the electromechanical behavior of a piezoelectric actuator bonded to a semi-infinite host structure with a partially debonded adhesive layer between them will be presented in this thesis. The actuator is modeled as a classical beam with an applied axial force. The bending effect of the actuator will be involved and the normal stress along the interface of upper and lower surfaces of adhesive layer are considered. The different geometrical parameters and material mismatch of the actuator system and the partially debonding condition are also investigated.

1.2 Research objectives

It is the objective of the current thesis to develop a piezoelectric actuator model involving the bending effect and partial debonding with an adhesive layer under static loads. Specifically, the detailed objectives of this research are identified as :

(1) establishing a new piezoelectric actuator model that is a thin-sheet piezoelectric layer bonded to an elastic semi-infinite host structure through an adhesive layer between them;

(2) conducting analytical and numerical analysis to investigate the electromechanical behaviour of debonding with bending effect under the static loading;

(3) investigating the effects of the different geometrical and material parameters of the system, especially that of the imperfect adhesive layer, upon the coupled response of the actuator.

1.3 Outline of the thesis

This thesis is organised into six chapters.

The current chapter provides the background, motivation and objectives.

The review of the state of the art of the relevant studies is presented in chapter 2.

In chapter 3, a modified model of partially debonded piezoelectric actuator with bending deformation and an adhesive layer is presented.

In chapter 4, the theoretical solutions of the actuator are presented, based on the use of

singular integral equations and Chebychev Polynomial expansion.

In chapter 5, FEM simulations are conducted and the analysis of adhesive layer are presented. The results of current model are compared with existing results under some different cases. The influences of the geometry and the material mismatch upon the electromechanical behaviour of the actuators are discussed in detail.

Chapter 6 summarizes a set of final conclusions and contributions, and recommendations are suggested for future studies.

Chapter 2: Review of the state of the art

This chapter gives the review of the state of the art of the piezoelectric actuator/sensors studies. Firstly, the brief history of the piezoelectricity and piezoelectric devices is discussed. Then, the modelling and analysis of the piezoelectric sensors/actuators to date are presented. The last section will present the applications of the piezoelectric actuator in the structural health monitoring (SHM).

2.1 History of piezoelectricity and piezoelectric devices

The past several decades have witnessed rapid progress in the engineered material structures with various functionalities (Li and Wang, 2016; Li et al., 2018, 2019; Wang, 2014). The exploration of piezoelectric materials serves as one of the most lasting and stimulating field of material research. Piezoelectric materials involve the interaction between the mechanical and electrical behaviour of the objects. This kind of materials possess mechanical-electrical and electrical-mechanical energy conversions properties. It can generate electrical charge when subjected to mechanical loads, referred to as the direct piezoelectric effect. The converse effect illustrates that an applied electrical field can generate mechanical deformation (Yang, 2006).

The direct piezoelectric effect was discovered by French physicists brothers Jacques and Pierre Curie in 1880 and they demonstrated the piezoelectric phenomena through systematic experiments on specially prepared tourmaline crystals. This effect was quickly termed piezoelectricity by Hankel to distinguish it from other areas of scientific phenomeno-

logical experience such as "contact electricity" and "pyroelectricity". However, the Curie brothers didn't predict the converse piezoelectric effect. In 1881, Lippman mathematically proved this property by using fundamental thermodynamic principles. Soon thereafter, Curie brothers confirmed the existence of the piezoelectric converse effect through experiment, and the quantitative proof of the complete piezoelectric effects was obtained later. Simultaneously, the piezoelectric effects were discovered in other natural crystals, such as quartz, zinc blende, and Rochelle salt (tartaric acid) (Jaffe, 2012).

In the subsequent 25 years, many physicists endeavoured to develop an exact theory on the basis of thermodynamics in quantifying complex relationships among mechanical and electrical variables. In 1910, Voigt first gave comprehensive explanation of the complex relationship in his published work. Since the underlying mathematics was very complicated, piezoelectricity didn't catch much attention at that time, lacking practical applications. Until the World War I, piezoelectricity had the first important application. In 1917, P. Langevin developed the first ultrasonic submarine detector and the transducer included a thin quartz crystal sandwiched between two steel plates. The plates could launch ultrasound waves into the water after the quartz crystal was excited. Then, the second quartz device was used to detect the return of the sound wave. Based on the time from launching pulse to returning, the depth of the submarine could be determined. Their success made piezoelectric materials possible to apply into other aspects except for underwater application such as ultrasonic transducers, microphones, and accelerometers. However, the available materials at that time were natural crystals with piezoelectric properties, which limited performance of the device and the related commercial applications.

The second breakthrough for piezoelectric material happened in World War II. The first ceramic material, barium titanate (BaTiO3), was discovered by different groups from the US, Japan and Soviet Union separately in 1943. This kind of material could increase dielectric constants up to 100 times larger than natural crystals. Furthermore, another man-made material called the ferroelectric was manufactured to have similar improvements in piezoelectric properties. These discoveries sped up research and development of numerous ceramic piezoelectric materials. Among these discoveries, the most notable ones were the findings of lead metaniobate (PMN) and lead zirconate titanate (PZT) in 1950s. Compared with natural piezoelectric crystals, they can be made in almost any shape or size thanks to their ceramic nature. Since then, these kinds of materials have been exploited in a wide range of applications, such as actuators, sensors and transducers in structural health monitoring, intelligent structures, noise, shape and vibration controls etc.

2.2 Modelling and analysis of piezoelectric sensors/actuators

The piezoelectric actuators and sensors provide a good approach to obtain an active control strategy. Over the past several decades, in order to study the coupled electromechanical behaviour and static load transfer between the piezo-actuator and the host structure, researchers have proposed different modelling approaches. Piezoelectric thin films are usually bonded to the surface of the host structure. The majority of the available methods can be categorized into three classes, namely analytical, numerical and hybrid approaches.

The first category is the analytical approach. Analytical models include the pin-force model, the beam-theory-based-model, the piezoelectric plates and shells models and the

elasticity equation-based model. The pin-force model is one of the earliest models developed for beams actuated in bending. This model treats the actuators and host substrate as separate elastic bodies and the transferred forces from the actuator to the substrate are through "pins" at the edges of the actuators, which means shear stress is concentrated in a small area. Baily (Bailey and Hubbard, 1985) firstly established this kind of model, in which a thin piezoelectric polymer was bonded to one side of the cantilever beam, with only the transverse vibrations of the beam being analyzed. Although this model worked well in perfect bonding scenario, it failed to provide correct structural response when the actuator was relatively thick. Crawley and De Luis (Crawley and De Luis, 1987) firstly proposed a comprehensive static model of the interaction between the thin piezoelectric actuators bonded to or embedded in beam-like structures. This model assumed uniform axial strain across the actuator and the host structure was treated as a Euler-Bernoulli beam. Later, Crawley and Andeson (Crawley and Anderson, 1990) presented a model assuming both structure and actuators undergoes consistent Euler-Bernoulli strain, which is the linear strain distribution across the actuator. This model could illustrate the induced extension, bending, and localized shear deformations. For further modifications, Im and Atluri (Im and N. Atluri, 1989) took into account the effects of transverse shear and axial forces as well as a bending moment in the beam (Crawley and De Luis, 1987). Ziya KK et al. (Kusculuoglu et al., 2002) extended the Euler-Bernoulli beam models to Timoshenko beam models by considering the shear deformation and the rotary inertia.

Plate and shell models have also been extensively developed in modelling the piezoelectric sensors/actuators. The earliest model of plate could date back to the year 1952.

Mindlin (Mindlin, 1952) gave an approximate theory of the piezoelectric crystal plates in thickness-shear and flexural modes, which involved the early terms of series expansions of the mechanical displacement and electric potential. Then, an exact solution for static analysis of simply supported laminated piezoelectric plate using double Fourier series was obtained (Mindlin, 1972). Dimitriadis et al. (Dimitriadis et al., 1991) designed a model with a two-dimensional thin piezoelectric patches bonded to the opposite plate surfaces. They investigated the static and dynamic cases. The results showed the potential for controlling vibration in distributed systems. Mitchell and Reddy (Mitchell and Reddy, 1995) derived the theories for laminated piezoelectric plate using the classical plate theory and the third-order shear deformation theory. M. Rahmoune et al. (Rahmoune et al., 1998) developed a new thin piezoelectric plate model and analyzed its mechanical behaviour by using a mathematical asymptotic approach. Tzou and Gadre (Tzou and Gadre, 1989) derived the equations of motion of the generalized multi-layered thin piezoelectric shell by using Hamilton's principle. Then, they developed a new theoretical model with thick anisotropic composite piezoelectric shells made of multi-layered triclinic piezoelectric laminates by assuming that each layer was perfectly bonded together to become a single thick piezoelectric laminate system. A composite piezolaminated shallow thin shell theory was developed (Miller and Abramovich, 1995), in which the individual laminate is capable of electromechanical transduction. The theoretical parameters of segmented transducers laminated on a piezoelectric cylindrical shell were analyzed (Tzou et al., 1996). The dynamic behaviour of piezoelectric shells was investigated by (K Chai and Arnold, 2006; Tzou et al., 2002) and the piezoelectric shells have applications in aerospace technology, such as rocket nozzles. The three-dimensional vibration characteristics of coupled motions for piezoelectric

cylindrical shells with free boundary conditions were investigated by using three different experimental methods and finite element numerical modeling. A latest review on modeling of piezoelectric integrated plates and shells can be found (Zhang et al., 2019). In the models mentioned above, the integrated structures were modelled as beams, plates or shells. In what follows, only the global responses of the whole systems were focused without the local information. As a result, these models were not suitable for predicting local stress distribution near the ends of the actuators.

The elasticity equation-based model can provide an alternative choice for the main interest of local stress concentration and the load transfer near the actuator. When a thin-sheet piezoelectric actuator is embedded into or bonded to an elastic structure, the host structure can be assumed to be semi-infinite which is governed by the equations of elasticity. Because the thickness of an actuator is usually much thinner than the host structure. Wang and Meguid (Wang and Meguid, 2000) first developed an analytical model featuring the static coupled electromechanical behaviour with a thin piezoceramic actuator embedded in or bonded to an elastic medium under inplane mechanical and electrical loadings, in which the local stress distribution and load transfer near the actuator were studied. This work was further extended and modified by Jin and Wang (Jin and Wang, 2011b) to investigate the effect of the bonding layer between the actuator and the host structure. The analytical results of these models are in good agreement with the corresponding finite element results. But these kind of models just characterize the shear stress along the interface, so they don't provide information on the normal stress between the piezoelectric layer and the host structure. This thesis will provide a model of a thin-sheet piezoelectric actuator bonded

to a semi-infinite host structure with an adhesive layer between them and investigate the coupled electromechanical behaviour, in consideration of the bending deformation of the piezoelectric actuator and partial debonding along the interface.

Numerical approaches have also been widely utilized to analyze the electromechanical behaviour induced by the piezoelectric actuators (Allik and Hughes, 1970; Ha et al., 1992; Hwang and Park, 1993; Tzou and Tseng, 1990). In modelling piezoelectric actuators, some commercial finite element software, e.g., COMSOL Multiphysics and ANSYS, provide researchers convenient tools to simulate coupled physical behaviour. A.benjeddou (Benjeddou, 2000) surveyed and discussed the advances and trends in the formulations of finite element modeling of piezoelectric-based structure. The modelling approaches of piezeoelectric actuators bonded to an elastic medium have been demonstrated and the disadvantages of FEM simulations as follows (Huang et al., 2010). First, it can't provide a direct insight into the physical structures for targeted parameters. Besides, a classical FEM model is not applicable to infinite open waveguides since it works within spatially restricted discretization domains (Glushkov et al., 2007). The last one is that unaffordable computational costs are usually required due to a slow convergence for obtaining the responses of a three-dimensional model at high frequencies. Hybrid approaches which combine FEM with analytical approaches were proposed to compensate for the disadvantages of pure FE simulations. In this approach, the analytical methods are mainly utilized for the host structures, and the FE methods are mainly used for the remaining structures of the system. The hybrid schemes consume less computational efforts because the host structure model usually have much more elements than actuator model. However, this approach still can't

provide a direct insight of the physical explanation of the calculated results (Huang et al., 2010).

2.3 Modelling of the partial debonding of piezoelectric actuators

In the previous section, the perfectly bonded layers conditions have been discussed. However, the damage initiation and propagation occur in a series of events when a load is applied to a laminated composite. There are three principal damage modes in a composite laminate, which are interlaminar matrix delamination, intra-ply cracking and fiber failure (Garg, 1988). Among these failure modes, the interlaminar matrix delamination is one of the most serious failure modes. Due to the substantial in-plane residual compressive stress, the delamination along the interface of the piezoelectric actuator and the host structure happen. The delamination is defined as a debonding or separation between individual layers of the laminate when subjected to in-plane loads. As a result, it may affect some design parameters like natural frequencies and mode shapes (Della and Shu, 2007).

A considerable amount of analytical models and numerical analysis have been reported for modelling the partial debonding of the piezoelectric actuators. Seeley and Chattopadhyay (Seeley-C-1998) investigated the significant effect of the partial debonding at the piezoelectric actuator and smart composite laminates interface on the dynamic response. The experimental results showed good agreement with the previous numerical results (Seeley and Chattopadhyay, 1996). Wang and Meguid (Wang and Meguid, 2000) developed the solutions of the edge debonding and the central debonding of the piezoelectric layer, which is bonded on an elastic semi-infinite host under plane strain loading. Then, several

analytical models for a smart beam with a debonded piezoelectric actuator by using the region approach and classical beam theory have been presented (Liyong et al., 2001b; Sun et al., 2001; Tylikowski, 2001b). For the debonding region, it was assumed that there was no stress transferring between the piezoelectric actuator and the host beam. Using similar assumptions, Luo and Tong (Luo and Tong, 2002a,b) got the the exact static solutions numerically and analytically, which included the normal stress for a PZT composite beam with adhesive layers. A closed-loop control based damage detection scheme was presented to detect debonding of a piezoelectric actuator patch from its host structure. The simulation results showed that even a very small debonding length can destabilize the control system. Then, the shear lag effect on the impedance formulations was analyzed and the results illustrated that the bonding layer could modify the measured electromechanical admittance (Bhalla and Bajaj, 2008). The existing analytical models and numerical analysis of the delaminated composite laminates with piezoelectric sensors/actuators have been intensively reviewed (Della and Shu, 2007). A model with a partially debonded piezoelectric actuator in smart laminates was proposed by using layerwise displacement field (Huang et al., 2015). Recently, a theoretical model of a thin piezoelectric actuator bonded to a graded half plane with an adhesive layer is analyzed (Chen et al., 2018a,b).

2.4 The investigation of the effects of the adhesive layer

In order to precisely detect the vibrational behaviour of smart structures using PZTs, piezoelectric sensors and actuators need to be attached to the structure. One of the commonly utilized ways is to attach the piezoelectric layers on the surface of the structure by using adhesives since adhesives do not change material properties of the target structure (Kwak

and Sciulli, 1996; Shen, 1994). However, It has been reported that the vibration controllability of smart structures may suffer when the mechanical properties of adhesive layers are ignored in the dynamic model of the smart structures (Akella et al., 1994; Nakra, 1998; Prakah-Asante and Craig, 1994).

In the works which considered mechanical properties of adhesives in their structural models, the effects of three different adhesives on the vibration damping properties of composite beams was investigated (Park et al., 2000c). The influence of the adhesive layer parameters on the active damping response of the controlled beams was analyzed (Pietrzakowski, 2001). In this study, the adhesive layers were assumed as visco-elastic materials and only the longitudinal extension of the piezoelectric layer and the adhesive layer was considered. The frequency response of the system showed that the stiffness of the adhesive layers significantly affected the active damping efficiency. The interfacial stress increased greater near the sensor ends for a stiffer bonding layer than a soft bonding layer.

A different approach for the modelling of a closed-loop vibration control of a smart beam with adhesive layers, piezoelectric sensor and actuator patches was presented (Sun et al., 2001). Although the normal and shear strains of the adhesive layer were taken into account, these strains were assumed to be constant along the thickness of the adhesive layer. Then, the influence of the mechanical and geometrical properties of the adhesive layer on the static response of the active structure was analyzed by utilizing the high-order theory (Rabinovitch and Vinson, 2002b). The adhesive layers were modelled as a two-dimensional linear elastic media with shear and vertical stresses in consideration. The sensitivity study results revealed that the geometries and the material properties of the adhesive layers could

influence the response of the piezoelectric patch. Thus, proper selection of the adhesive layers properties can enhance the performance of such smart structures. The impact of the bonding quality of the adhesive layer on the sensing capability of piezoelectric sheets was addressed (Faria, 2003). The adhesive layer was assumed to be elastic and in a pure shear stress state, which is between the piezoelectric material and the host structure. The results of this two-dimensional FE model showed that the shear lag effects due to edge effects on the strain distributions and end-bonding needed to be carefully assessed in order to improve the sensing efficiency of piezoelectric sensors.

The interfacial debonding behaviour of composite beams with a piezoelectric layer, an adhesive layer and a host beam was studied (Liang et al., 2010; Wang et al., 2013). The piezoelectric layer and the host beam were modelled as Timoshenko beams; the adhesive layer was modelled as a continuous spring with shear and peel stiffness. The analytical electromechanical solutions for the adhesively bonded composite single-lap joints were presented using the full layerwise method (Yousefsani and Tahani, 2013). The accuracy and effectiveness of the model were verified by the corresponding numerical and experimental results. The same approach was utilized to investigate the void edge effects (Yousefsani and Tahani, 2018). It was observed that there were high interfacial stress concentration around the void edges.

All of the aforementioned works are based on limited thickness of the host structures. Lu and Wang (Han et al., 2008a,b) examined the effect of the adhesive layer on the coupled dynamic behaviour of a thin piezeolectric sensor and actuator bonded to an elastic medium under inplane mechanical and electrical loadings. The shear stress deformation was dis-

cussed. However, the normal stress distribution was not considered. The analytical results indicated that the modulus and the thickness of the bonding layer have significant effects on shear stress distribution. The static electromechanical behaviour of the piezoelectric sensor/actuator was analyzed later (Jin and Wang, 2011a,b). The results showed that the analytical results and those of finite element simulations were in a good agreement. However, the normal stresses in the adhesive layer and the bending effects in the piezoelectric layer were neglected in the whole invetigation.

2.5 Applications of piezoelectric sensors/actuators in structural health monitoring (SHM)

The piezoelectric material as a kind of smart material can convert mechanical energy into electrical energy and vice versa. This reciprocal energy transforming capability enables the materials to function as sensors, actuators or transducers. Owning to its unique electromechanical coupling effects, together with some other good characteristics such as light weight, distributed characteristics, high coupling factor, quick response, low energy consumption and low cost, piezoelectric actuators/sensors have been utilized in a wide range of applications, which include piezoelectric ultrasonic motors (Milsom et al., 1977; Monkhouse et al., 2000; Staszewski et al., 2009), vibration control or noise suppression using piezoelectric layer (Choi and Han, 2016; Ha et al., 1992; Wang et al., 2001), energy harvesting (Calio et al., 2014; Kim et al., 2011), and piezoelectric transducers for structural health monitoring (SHM) (Tua et al., 2004, 2005).

SHM, as one of the most typical applications of the piezoelectric materials, has re-

ceived increasing attention from the researching community and the industry in the past several decades. It aims at detecting damages and providing a diagnosis of structural health. Many researchers have explored the built-in sensor network-based structural health monitoring for rapid non-destructive evaluation in real time and provide long-term monitoring of structural health status. In general, there are two existing techniques based on piezoelectric transducers. Electromechanical impedance based technique for near-field damage and wave propagation based for far field damage have been developed.

2.5.1 Electromechanical impedance (EMI) based technique

Electromechanical impedance (EMI) based technique is a relatively new non-destructive testing method. The mechanism of this technique is to utilize a single PZT transducer, which acts as an actuator and a sensor, simultaneously. The PZT patches just require a very low level voltage, typically less than 1 V, to produce a very high frequency excitation in the host structure. This will cause the host to vibrate, which makes the PZT to generate a current to flow through the PZT transducer. Any changes in the vibration behaviour of the host structure will be reflected in terms of the electrical admittance signatures across the PZT patch.

In the pioneering theoretical research of the EMI based on technique, a one-dimensional model was presented, which showed that the electrical admittance of the PZT was directly related to the mechanical impedance of the structure (Liang et al., 1994). Then, a frequency domain impedance-based technique for health monitoring was developed (Sun et al., 1995). This newly technique could act as a promising tool for real-time structural damage assessments by testing an assembled truss structure.

Numerous researchers utilized the EMI technique for structural health monitoring, to detect and examine the severity of damages in a variety of systems. Experimental investigation were carried out by Park et al. (Park et al., 2000a) and the results showed the capability and effectiveness of EMI in monitoring damages on various civil structures. Monitoring of a prototype reinforced concrete (RC) bridge structure had been performed by Soh et al. (Soh et al., 2000). The feasibility of using PZT patches for monitoring the real time health of the critical regions of real-life civil structural systems had been demonstrated. Victor and Andrei (Giurgiutiu and Zagrai, 2005) have used the impedance method for health monitoring of thin plates and aerospace structures. An investigation has been conducted to utilize the impedance method in identifying structural damage in space systems and satellites in particular, with the factors affecting realization of the SHM system discussed (Zagrai et al., 2010). The EMI based techniques have also been introduced to the field of biomechanics for non-invasive assessment of the dental implants stability (Boemio et al., 2011; Ribolla and Rizzo, 2015). The comprehensive reviews on the engineering SHM applications of the EMI based techniques have been conducted (Annamdas and Soh, 2010; Mei et al., 2019; Na and Baek, 2018b; Park et al., 2003; Qing et al., 2019; Yang et al., 2008).

Despite of its widely used applications, the EMI based technique is a near-field damage detection method that uses high frequency excitation. To develop an efficient SHM system detecting near-field and far-field damages, another method should be incorporated. The EMI technique and the guided wave-based technique had been used simultaneously for structural-interrogation and damage detection (Giurgiutiu et al., 2002, 2004). The study showed that the EMI technique was found to be very sensitive for assessing the health of

a near field while the guided wave based technique was more suitable for far-field damage detection.

2.5.2 The wave propagation (WP) based technique

The wave propagation (WP) based technique, as one of practical NDE techniques for structural health monitoring, has also attracted much attention (Bourasseau et al., 2000; Ghosh et al., 1998; Tan et al., 1995). The WP technique employs two or more piezoelectric transducers, which can be embedded into or bonded onto the host structure. Utilizing the piezoelectric effects, one transducer acts as an actuator to generate pre-selected diagnostic signals, and the other transducers serve as sensors to collect the diagnostic signals, which contains the information of the size and location of the damage or the material property changes within the structure. This is due to the fact that any structural property change along the travelling path of the induced elastic waves will be reflected in the changes of electrical signatures (Giurgiutiu, 2007; Ihn and Chang, 2004; Yu and Giurgiutiu, 2008).

To date, a large number of WP based technique studies have been carried out. The wave propagation method originally was proposed by Chang et al. (Wang and Chang, 1999). In the WP based technique, guided waves, such as Lamb and Rayleigh waves, are mainly used for damage detection in metallic structures and composite structures. Moulin et al. (Moulin et al., 2000) presented a modeling technique for lamb waves transducers attached to or embedded in composite plates. The applicability of the model was validated with experimental study. A piezoelectric based built-in diagnostic technique for monitoring crack growth in metallic structures was presented by Ihn and Chang (Ihn and Chang, 2004). Giurgiutiu derived a model of plane harmonic Lamb waves tuning mechanism with

piezoelectric transducers (Giurgiutiu and Zagrai, 2005). Then, a series of one-dimensional and three-dimensional modeles involving piezoelectric generated guided waves propagating in thin metallic strip was presented (Giurgiutiu, 2007). Recently, the applications of the WP technique have been extended to concrete structures, including damage monitoring (Lim et al., 2018; Lu et al., 2013), concrete hydration (Lim et al., 2016; Tawie and Lee, 2011) and strength monitoring (Gu et al., 2006; Song et al., 2008).

Although the wave can propagate over long distances in a structure, the major difficulties to conduct a nondestructive test using the wave propagation based technique are dispersive properties of waves, existing of multiple wave modes at a given frequency (Alleyne and Cawley, 1992) . These difficulties have resulted in substantial efforts to study about the interaction between piezoelectric material layers and host structures, and the resulting complicated electromechanical behaviour in a SHM system (Wang and Mai, 2002; Xu et al., 2015).

Chapter 3: Modelling of the piezoelectric actuator with an adhesive layer

3.1 Introduction

This chapter develops a new model of thin-sheet piezoelectric actuators bonded to the surface of a homogenous and isotropic semi-infinite elastic structure with an adhesive layer between them, under in-plane electrical loading to study its coupled electromechanical behaviour. The current model is an extension of the work presented in Wang and Meguid (2000), where the piezoelectric actuator is modelled as an electro-elastic line subjected to a transverse electric field with its poling direction perpendicular to its length. In this study, the possible partial debonding of the piezoelectric actuator is simulated through an imperfectly bonded adhesive layer. The Euler-Bernoulli beam theory is utilized for describing the behaviour of the actuator, and the adhesive layer is modelled as a continuous spring with the shear and normal moduli. The model developed in this chapter provides the theoretical formulation of the problem for the further analysis and discussion in the following chapters.

3.2 The piezoelectric actuator model

3.2.1 The assumptions and governing equations

Consider the problem of a thin piezoelectric actuator layer bonded to a homogeneous and isotropic elastic structure on the top surface through an adhesive layer, as illustrated in figure 3.1. The dimension of the piezoelectric actuator is much smaller than that of the structure, which makes the modelling of the structure as a semi-infinite medium valid. Also, plane strain deformation is assumed due to the fact that the width of the actuator is significantly large in comparison with its thickness in this model. As shown in figure 3.1, the thickness and length of the actuator are denoted by h and $2c$, respectively. The thickness of the adhesive layer is h'. It should be mentioned that to simplify the formulation, without loss of generality, the structure is assumed to have unit width in this study. The origin of the coordinate system is located at the center of the interface of the host structure and adhesive layer, and the so-called poling direction of the actuator is along z-axis, i.e. the thickness direction. An electric potential V is applied between the upper and lower electrodes of the piezoelectric actuator and the resulting magnitude of the electric field can be expressed as

$$E_z = -\frac{V}{h} = \frac{(V^- - V^+)}{h}, \tag{3.1}$$

where V^+ and V^- stand for the electric potentials at the upper and lower surfaces of the piezoelectric actuator, respectively, as illustrated in figure 3.1. In this study, the subscripts p, a and s are used for representing the piezoelectric actuator layer, the adhesive layer, and the host structure, respectively.

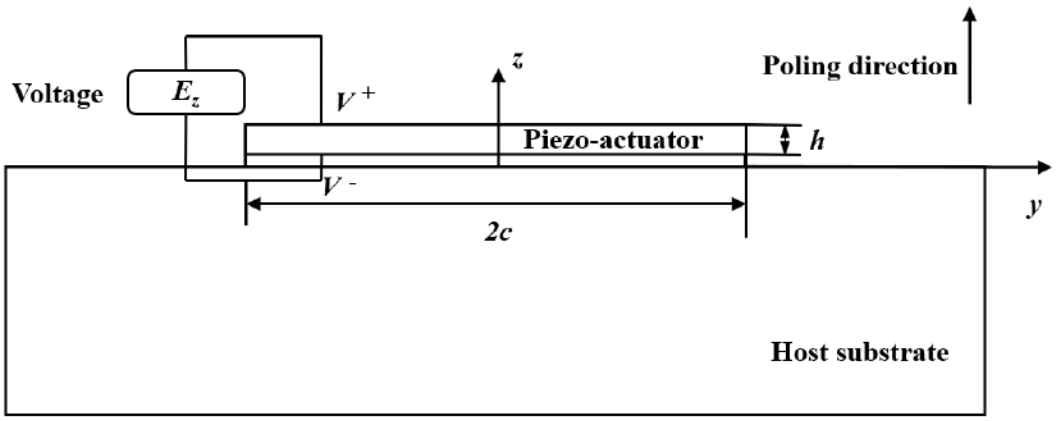

Figure 3.1: Schematics of the actuator configuration.

Figure 3.2 depicts the free-body diagram of the infinitesimal actuator, adhesive layer and the host structure with N, Q and M being the resultant axial force, the transverse shear force and the bending moment, respectively. In light of the structural feature of the actuator, the following assumptions can be made. Firstly, the average axial stress σ_y^p and the displacement u_y^p in the actuator can be assumed to be uniform across the thickness of the actuator. Secondly, these stresses in the actuator, σ_z^p and σ_{yz}^p, can be ignored. Thirdly, the shear stress τ and normal stress σ transferred along the interface between the piezoelectric actuator and the adhesive layer will act as distributed body forces for the actuator. In what follows, the piezoelectric actuators can be modelled as an electro-elastic Euler-Bernoulli beam undergoing longitudinal and transverse deformations, which is subjected to an uniform electric field E_z and distributed axial and transverse forces, τ/h and σ. While, the adhesive layer is assumed to only carry shear and normal stresses. Based on the above

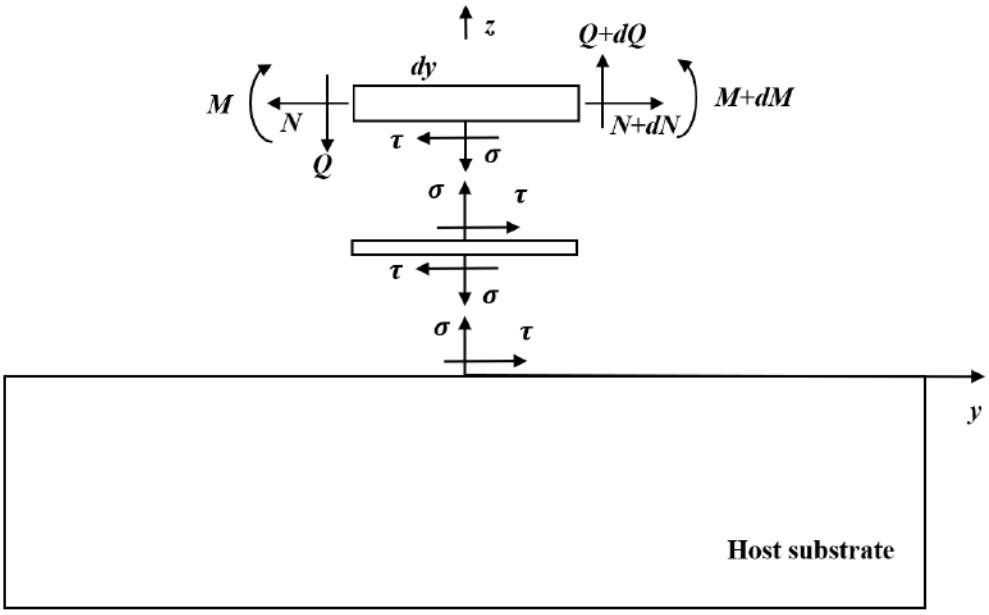

Figure 3.2: Free-body diagrams of the piezoelectric actuator, adhesive layer and the host structure.

assumptions, the equilibrium equations of the actuator can be obtained as

$$dN - \tau dy = 0, \ \left(\sum F_y = 0\right), \tag{3.2}$$

$$dQ - \sigma dy = 0, \ \left(\sum F_z = 0\right), \tag{3.3}$$

$$dM + Qdy = 0, \ \left(\sum M = 0\right). \tag{3.4}$$

Based on the force stress relation $dN = hd\sigma_y^p$, the governing equations can be converted into

$$\frac{d\sigma_y^p}{dy} - \frac{\tau}{h} = 0, \tag{3.5}$$

$$\frac{d^2M}{dy^2} + \sigma = 0. \tag{3.6}$$

The average axial stress σ_y^p in the actuator can be expressed through the integration of

equation (3.5) as

$$\sigma_y^p(y) = \int_{-c}^{y} \frac{\tau(\xi)}{h} d\xi + \overline{c}, \tag{3.7}$$

where $\overline{c}$ is an unknown constant, which can be solved with the boundary condition at the ends of the piezoelectric actuator. Also, the bending moment in terms of the transverse displacement component u_z^p will be in the form of

$$M = E^p I \frac{d^2 u_z^p}{dy^2}, \tag{3.8}$$

with I and E^p being the moment of inertia and the effective Young's modulus of piezoelectric actuator, respectively.

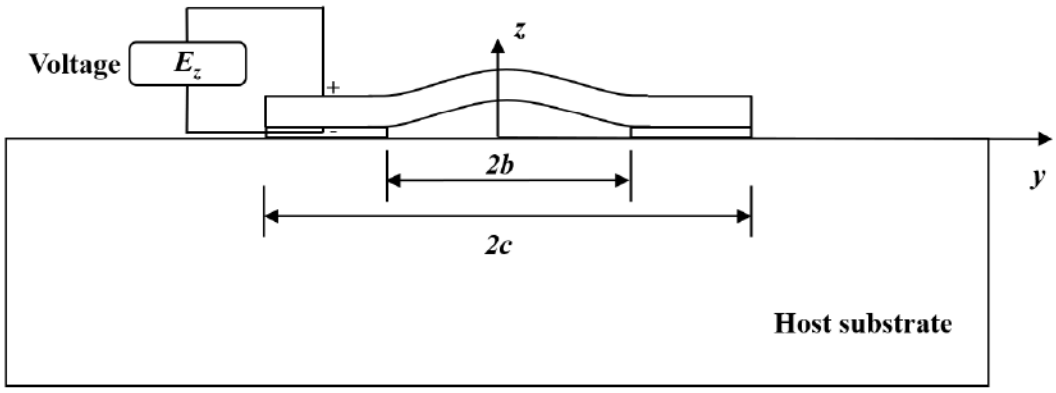

Figure 3.3: Schematics of the actuator configuration with partial debonding.

Generally, high localized stress concentration or poor interfacial conditions may result in the partial debonded region along the interface of two layers, which may consequently change the load transfer at the interface. Figure 3.3 illustrates the case of the piezoelectric actuator with partial central debonding in $|y| < b$, where, b represents the half length of the debonded part. In this case, the effective length of the actuator is reduced to $(2c - 2b)$. Traction free condition is assumed along the surfaces of the debonded interfaces, the possi-

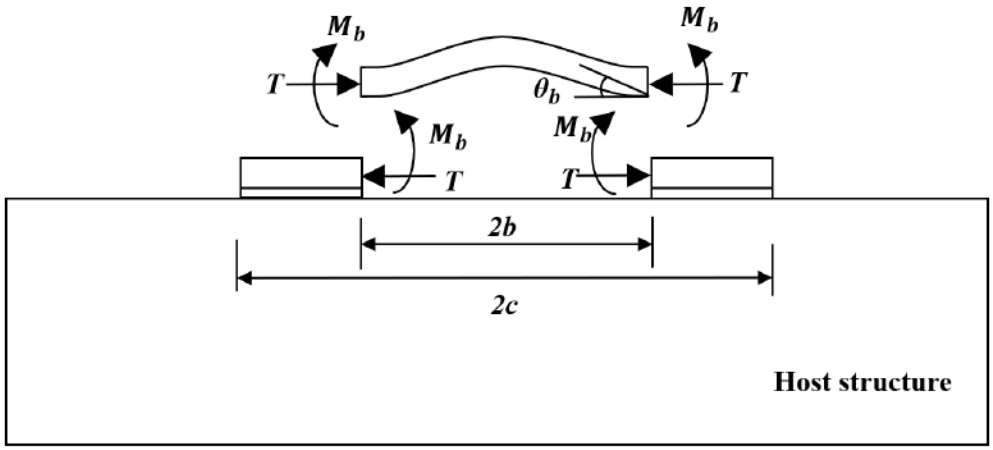

Figure 3.4: Free-body diagrams of the piezoelectric actuator with partial debonding.

ble contact of which is ignored for simplicity. In the bending state, the ends of the debonded part of the piezoelectric actuator $|y| = b$ are subjected to a resultant compressive force, T, and a moment, M, as shown in figure 3.4.

3.2.2 Constitutive relations of the actuator

According to the electro-elastic line piezoelectric actuator model under plane strain condition (Wang and Meguid, 2000), the related constitutive relation can be described as

$$\sigma_y^p(y) = E^p \varepsilon_y^p(y) - e_{31}^p E_z, \tag{3.9}$$

where E^p and e_{31}^p are the effective piezoelectric constants. These effective material constants are given by

$$E^p = c_{11} - \frac{c_{13}^2}{c_{33}}, \quad e_{31}^p = e_{31} - e_{33}\frac{c_{13}}{c_{33}}. \tag{3.10}$$

The detailed mathematic procedure can be found in Appendix A.

3.2.3 Boundary conditions

The traction free boundary condition at the two ends of the piezoelectric layer will result in zero bending moment and zero transverse shear force, namely,

$$\sigma_y^p = 0, \quad M = 0, \quad Q = 0, \quad at\ |y| = c. \tag{3.11}$$

Since this study is focused on a thin sheet piezo-actuator, the transverse shear force at the end of debonded part is assumed to be zero, as shown in figure 3.4. These boundary conditions at the bebonded part are expressed as

$$\sigma_y^p = -\frac{T}{h}, \quad M = M_b, \quad Q = 0, \quad at\ |y| = b; \tag{3.12}$$

$$u_z^p = u_{zb}^p, \quad \frac{du_z^p}{dy} = -\theta_b, \quad at\ |y| = b; \tag{3.13}$$

where T stands for axial compressive force in the debonded part and M_b represents the bending moment at the ends of debonded part, as shown in figure 3.4. There is no stress transferring between the piezoelectric actuator and the host structure in the debonded part, where $\sigma = 0$ and $\tau = 0$ can be expected. At the center of the debonding section, symmetry of the structure indicates the following the boundary conditions,

$$\frac{du_z^p}{dy} = 0, \quad \frac{d^3u_z^p}{dy^3} = 0, \quad at\ y = 0. \tag{3.14}$$

3.2.4 General solution for the actuator

Substituting the average axial stress σ_y^p in equation (3.7) into constitutive equation (3.9), the axial strain ε_y^p in terms of the interface shear stress $\tau(y)$ can be written as

$$E^p \varepsilon_y^p(y) = \int_{-c}^{y} \frac{\tau(\xi)}{h} d\xi + e_{31}^p E_z + \bar{c}. \tag{3.15}$$

At the left end of the piezoelectric actuator, $y = -c$, the axial stress is named as σ_{yl}^p. According to equation (3.7), it is equal to $\bar{c}$ in value. Equation (3.15) can then be rewritten as

$$E^p \varepsilon_y^p(y) = \int_{-c}^{y} \frac{\tau(\xi)}{h} d\xi + e_{31}^p E_z + \sigma_{yl}^p. \tag{3.16}$$

Similarly, at the right end of the actuator, $y = c$, the axial stress is named as σ_{yr}^p and it can be expressed as

$$\sigma_{yr}^p = \sigma_{yl}^p + \int_{-c}^{c} \frac{\tau(y)}{h} dy. \tag{3.17}$$

Then, from equations (3.16) and (3.17), the axial strain can also be expressed as,

$$E^p \varepsilon_y^p = e_{31}^p E_z + \sigma_{yr}^p - \int_{y}^{c} \frac{\tau(\xi)}{h} d\xi. \tag{3.18}$$

Traction free conditions at the ends of the actuator lead to

$$\sigma_{y1}^p = \sigma_{yr}^p = 0. \tag{3.19}$$

In what follows, equations (3.16) and (3.18) can be rewritten as

$$E^p \varepsilon_y^p(y) = \int_{-c}^{y} \frac{\tau(\xi)}{h} d\xi + e_{31}^p E_z, \tag{3.20}$$

$$E^p \varepsilon_y^p(y) = e_{31}^p E_z - \int_y^c \frac{\tau(\xi)}{h} d\xi, \tag{3.21}$$

with

$$\int_{-c}^{c} \tau(y) dy = 0. \tag{3.22}$$

After central debonding occurs, the axial strain $\varepsilon_y^p(y)$ of the piezoelectric actuator can be determined in terms of the shear stress τ by making use of the boundary condition at point b, $\sigma_b^p = -T/h$,

$$\varepsilon_y^p(y) = \frac{1}{E^p h} \int_b^y \tau(\xi) d\xi + \frac{e_{31}^p E_z}{E^p} - \frac{T}{E^p h}, \quad b < y < c. \tag{3.23}$$

Combining equations (3.6) and (3.8) yields the transverse deflection of the piezoelectric actuator as a function of the interfacial normal stress,

$$\frac{d^4 u_z^p}{dy^4} = -\frac{\sigma(\xi)}{E^p I}. \tag{3.24}$$

To obtain the solution for bending deformation, successive integration is needed for the equation (3.24). First, the first integration of equation (3.24) is shown in

$$E^p I \frac{d^3 u_z^p}{dy^3} = -\int_b^y \sigma(\xi) d\xi - \overline{Q}, \quad b < y < c. \tag{3.25}$$

The integration of equation (3.25) results in the curvature of the actuator,

$$E^p I \frac{d^2 u_z^p}{dy^2} = -\int_b^y \int_b^\eta \sigma(\eta) d\eta d\xi - \int_b^y \overline{Q} d\xi + \overline{M}, \quad b < y < c. \tag{3.26}$$

The integration of equation (3.26) yields the slope of the piezoelectric actuator, which can

be expressed as

$$E^p I \frac{du_z^p}{dy} = -\int_b^y \int_b^\eta \int_b^\zeta \sigma(\zeta) d\zeta d\eta d\xi - \int_b^y \int_b^\eta \overline{Q} d\eta d\xi + \int_b^y \overline{M} d\xi + \overline{A}, \;\; b < y < c. \tag{3.27}$$

Based on the boundary condition illustrated in equation (3.12), $\overline{Q} = Q_b = 0$. Also, $\overline{M}$ is equal to the bending moment at point b, M_b. In what follows, the resulting slope of the piezoelectric actuator can be further written as

$$\frac{du_z^p}{dy} = -\frac{1}{E^p I} \int_b^y \int_b^\eta \int_b^\zeta \sigma(\zeta) d\zeta d\eta d\xi + \frac{M_b(y-b)}{E^p I} - \theta_b, \;\; b < y < c, \tag{3.28}$$

where $\theta_b = -\frac{du_z^p}{dy}|_{y=b}$ represents the slope of piezoelectric actuator at the point $y = b$.

Based on the relation between the bending moment and the deflection of the piezoelectric actuator illustrated in equation (3.8), the deflection angle θ_b of the debonded part can be determined in terms of the bending moment M_b at $y = b$ as

$$\theta_b = -\frac{M_b}{E^p I} b. \tag{3.29}$$

In addition, substituting axial stress σ_y^p in equation (3.12) into equation (3.9), the horizontal displacement at debonded point b can be expressed as

$$u_y^p|_{y=b} = \frac{e_{31}^p E_z h - T}{E^p h} b. \tag{3.30}$$

3.3 The adhesive layer

The adhesive layer between the piezoelectric actuator and the elastic structure is modelled as a continuous spring with both shear stiffness and normal stiffness. Due to the fact that all the mechanical response of the actuator is transferred through the adhesive layer, also, the

modulus of the adhesive layer is usually lower than that of the actuator and the host structure. So, the geometry and material properties of the adhesive layer may have significant effect upon the load transfer between the actuator and host structure.

Referring to figure 3.2 and using the constant shear strain assumption (Liyong et al., 2001a) along the thickness, the interfacial shear stress τ is determined by the stress-strain relation,

$$\tau = k_1(\Delta u_y) = k_1\left(u_y^a\left(y,h'\right) - u_y^a\left(y,0\right)\right), \tag{3.31}$$

where

$$k_1 = \mu^a/h', \tag{3.32}$$

with $\mu^a = \frac{E^a}{2(1+\nu^a)}$ being the shear modulus of the adhesive layer; Δu_y is interfacial displacement jumps between the actuator and the host structure. $u_y^a\left(y,h'\right)$ and $u_y^a\left(y,0\right)$ are the upper and lower surface longitudinal displacements of the adhesive layer, respectively. According to the continuity conditions of the displacements, $u_y^a\left(y,h'\right)$ and $u_y^a\left(y,0\right)$ also represent the longitudinal displacements of lower surface of the actuator and the upper surface of the host, respectively.

Using the similar assumption with uniform normal strain along the thickness, the normal stress σ along the interface also can be given as,

$$\sigma = k_2(\Delta u_z) = k_2(u_z^a\left(y,h'\right) - u_z^a\left(y,0\right)), \tag{3.33}$$

where

$$k_2 = \frac{E^a(1-\nu^a)}{(1+\nu^a)(1-2\nu^a)h'}, \tag{3.34}$$

with E^a and ν^a being the Young's modulus and Poisson's ratio of the adhesive layer; Δu_z is interfacial displacement jumps between the actuator and the host structure. $u_z^a(y,h')$ and $u_z^a(y,0)$ are the transverse displacement of upper adhesive layer and lower adhesive layer, respectively. According to the continuity conditions of the displacements, $u_z^a(y,h')$ and $u_y^z(y,0)$ also represent the transverse displacements of lower surface of the actuator and the upper surface of the host, respectively.

3.4 The host structure

The load transfer between the piezoelectric actuator and the host structure is realized through the interfacial normal and shear stresses. For the host structure, the boundary conditions are given as below

$$\sigma_{yz}^s(y,0) = \begin{cases} \tau(y), & b<|y|<c, \\ 0, & |y|>c, |y|<b, \end{cases} \qquad \sigma_z^s(y,0) = \begin{cases} \sigma(y), & b<|y|<c, \\ 0, & |y|>c, |y|<b. \end{cases} \tag{3.35}$$

The fundamental solution of a half elastic plane subjected to a horizontal concentrated force $d\tau$ and a vertical concentrated force $d\sigma$ at $y=0$ is (Muskhelishvili, 1953)

$$du_y^s(y,0) = \frac{d\sigma \mathrm{sgn}(y)}{2E^s}(1+\nu)(1-2\nu) - 2d\tau \ln|y| \frac{1-\nu^2}{\pi E^s}, \tag{3.36}$$

$$du_z^s(y,0) = -\frac{d\tau \mathrm{sgn}(y)}{2E^s}(1+\nu)(1-2\nu) - 2d\sigma \ln|y| \frac{1-\nu^2}{\pi E^s}. \tag{3.37}$$

Using the superposition principle, the resulting displacements along the interface from the transferring stresses can be obtained. Along the bonded range, $b<y<c$, the interfacial

axial displacement and transverse displacement in the host structure will be

$$u_y^s(y,0) = (\frac{1-2\nu}{1-\nu})\frac{1}{2\overline{E^s}}[\int_{-c}^{-b}\sigma(\xi)d\xi + \int_b^y \sigma(\xi)d\xi - \int_y^c \sigma(\xi)d\xi] \\ -\frac{2}{\pi\overline{E^s}}[\int_{-c}^{-b}\ln|y-\xi|\tau(\xi)d\xi + \int_b^c \ln|y-\xi|\tau(\xi)d\xi]. \tag{3.38}$$

$$u_z^s(y,0) = -(\frac{1-2\nu}{1-\nu})\frac{1}{2\overline{E^s}}[\int_{-c}^{-b}\tau(\xi)d\xi + \int_b^y \tau(\xi)d\xi - \int_y^c \tau(\xi)d\xi] \\ -\frac{2}{\pi\overline{E^s}}[\int_{-c}^{-b}\ln|y-\xi|\sigma(\xi)d\xi + \int_b^c \ln|y-\xi|\sigma(\xi)d\xi]. \tag{3.39}$$

Then, the interfacial axial displacement at the tip of debonded part b is

$$u_y^s(b,0) = -\frac{2}{\pi\overline{E^s}}\left[\int_{-c}^{-b}\ln\left|\frac{b-\xi}{\xi}\right|\tau(\xi)d\xi + \int_b^c \ln\left|\frac{b-\xi}{\xi}\right|\tau(\xi)d\xi\right]. \tag{3.40}$$

where $\overline{E^s} = E^s/(1-\nu^2)$ with E^s and ν being the Young's modulus and the Poisson's ratio of the host structure, respectively. Taking the first derivative of above displacements with respect to the horizontal axis, namely y axis, the corresponding strains resulting from the applied force can be expressed as

$$\frac{du_y^s(y,0)}{dy} = (\frac{1-2\nu}{1-\nu})\frac{1}{\overline{E^s}}\sigma - \frac{2}{\pi\overline{E^s}}\int_{-c}^{-b}\frac{\tau(\xi)}{y-\xi}d\xi - \frac{2}{\pi\overline{E^s}}\int_b^c \frac{\tau(\xi)}{y-\xi}d\xi, \tag{3.41}$$

$$\frac{du_z^s(y,0)}{dy} = -(\frac{1-2\nu}{1-\nu})\frac{1}{\overline{E^s}}\tau - \frac{2}{\pi\overline{E^s}}\int_{-c}^{-b}\frac{\sigma(\xi)}{y-\xi}d\xi - \frac{2}{\pi\overline{E^s}}\int_b^c \frac{\sigma(\xi)}{y-\xi}d\xi. \tag{3.42}$$

The strain at the tip of debonded part b caused by transverse displacement will be

$$\frac{du_z^s(b,0)}{dy} = -(\frac{1-2\nu}{1-\nu})\frac{1}{\overline{E^s}}\tau(b) - \frac{2}{\pi\overline{E^s}}\int_{-c}^{-b}\frac{\sigma(\xi)}{b-\xi}d\xi - \frac{2}{\pi\overline{E^s}}\int_b^c \frac{\sigma(\xi)}{b-\xi}d\xi. \tag{3.43}$$

3.5 Continuity conditions

To ensure continuity at the interface of the bonding parts, all displacements, interfacial stresses and strains must be identical. In what follows, the following continuity conditions are imposed,

$$\frac{du_y^p(y,h')}{dy} = \frac{du_y^a(y,h')}{dy}, \quad \frac{du_z^p(y,h')}{dy} = \frac{du_z^a(y,h')}{dy}, \quad b < |y| < c, \tag{3.44}$$

$$\frac{du_y^s(y,0)}{dy} = \frac{du_y^a(y,0)}{dy}, \quad \frac{du_z^s(y,0)}{dy} = \frac{du_z^a(y,0)}{dy}, \quad b < |y| < c. \tag{3.45}$$

Also, two additional continuity conditions of the displacements and strains at the tips of debonded part b need to be satisfied,

$$u_y^p(y,h') - u_y^s(y,0) = \frac{\tau(y)}{k_1}, \quad y = b, \tag{3.46}$$

$$\frac{du_z^p(y,h')}{dy} - \frac{du_z^s(y,0)}{dy} = \frac{d\sigma(y)}{dy}\frac{1}{k_2}, \quad y = b. \tag{3.47}$$

3.6 Formulation of the integral equations

Taking the derivative of both sides of equation (3.31) and (3.33) with respect to y yields

$$\frac{d\tau}{dy} = k_1\left(\frac{du_y^a(y,h')}{dy} - \frac{du_y^a(y,0)}{dy}\right), \tag{3.48}$$

$$\frac{d\sigma}{dy} = k_2\left(\frac{du_z^a(y,h')}{dy} - \frac{du_z^a(y,0)}{dy}\right). \tag{3.49}$$

According to the continuity equations (3.44) and (3.45), the above equations can be

rewritten as

$$\frac{d\tau}{dy} = k_1 \left(\frac{du_y^p(y,h')}{dy} - \frac{du_y^s(y,0)}{dy} \right), \tag{3.50}$$

$$\frac{d\sigma}{dy} = k_2 \left(\frac{du_z^p(y,h')}{dy} - \frac{du_z^s(y,0)}{dy} \right). \tag{3.51}$$

Substituting equations (3.23) and (3.41) into equation (3.50) in terms of the interfacial stress τ and σ, the following integral governing equation can be obtained

$$\begin{aligned} &\frac{2}{\pi \overline{E}^s} \int_{-c}^{-b} \frac{\tau(\xi)}{y-\xi} d\xi + \frac{2}{\pi \overline{E}^s} \int_{b}^{c} \frac{\tau(\xi)}{y-\xi} d\xi - (\frac{1-2\nu}{1-\nu}) \frac{1}{\overline{E}^s} \sigma(y) \\ &+ \frac{1}{hE^p} \int_b^y \tau(y) dy - \frac{T}{hE^p} + \frac{e_{31}^p E_z}{E^p} = \frac{1}{k_1} \frac{d\tau}{dy}, \end{aligned} \tag{3.52}$$

Substituting equations (3.28) and (3.42) into (3.51) leads to

$$\begin{aligned} &\frac{2}{\pi \overline{E}^s} \int_{-c}^{-b} \frac{\sigma(\xi)}{y-\xi} d\xi + \frac{2}{\pi \overline{E}^s} \int_{b}^{c} \frac{\sigma(\xi)}{y-\xi} d\xi + (\frac{1-2\nu}{1-\nu}) \frac{1}{\overline{E}^s} \tau(y) \\ &- \frac{1}{E^p I} \int_b^y \int_b^\eta \int_b^\zeta \sigma(\zeta) d\zeta d\eta d\xi + \frac{M_b(y-b)}{E^p I} + \frac{M_b}{E^p I} b = \frac{1}{k_2} \frac{d\sigma}{dy}. \end{aligned} \tag{3.53}$$

Substituting the continuity equation (3.46) at the debonded tip into the equations (3.30) and (3.40) get

$$\frac{2}{\pi \overline{E}^s} \left[\int_{-c}^{-b} \ln \left| \frac{b-\xi}{\xi} \right| \tau(\xi) d\xi + \int_b^c \ln \left| \frac{b-\xi}{\xi} \right| \tau(\xi) d\xi \right] + \frac{e_{31}^p E_z - T/h}{E^p} b = \frac{\tau(b)}{k_1}. \tag{3.54}$$

Similarly, based on the equation (3.47), the equations (3.29) and (3.43) can be reduced into

$$\frac{2}{\pi \overline{E}^s} \int_{-c}^{-b} \frac{\sigma(\xi)}{y-\xi} d\xi + \frac{2}{\pi \overline{E}^s} \int_{b}^{c} \frac{\sigma(\xi)}{y-\xi} d\xi + (\frac{1-2\nu}{1-\nu}) \frac{1}{\overline{E}^s} \tau(b) - \frac{M_b}{E^p I} b = 0. \tag{3.55}$$

In the four equations above, the four unknowns, i.e. the compressive force T, the bending moment M_b, the interfacial stresses σ and τ, are related, which has been illustrated as

$$\int_{-c}^{-b} \tau(\xi) d\xi = -T, \quad \int_b^c \tau(\xi) d\xi = T, \tag{3.56}$$

and

$$-\int_b^c \int_b^y \sigma(\xi) d\xi dy + M_b = 0, \quad -\int_b^c \sigma(\xi) d\xi = 0. \tag{3.57}$$

Equations (3.52) - (3.57) can be utilized to obtain the solution of this model, namely, the interfacial stresses τ and σ, the axial force T and the bending moment M_b at the ends of the debonded part of the actuator.

Chapter 4: Solution of the integral equations

4.1 Introduction

This chapter presents the analytical solutions of the governing integral equations for a piezoelectric actuator and an adhesive layer bonded to an elastic structure. The integral governing equations are solved mainly through two steps. Firstly, local coordinates are introduced to normalize the integral equations. Secondly, the solutions of the results singular integral equations are solved using Chebyshev polynomials expansions of the interfacial shear and normal stresses.

4.2 Normalized singular integral equations

In chapter 3, the governing integral equations for the coupled electromechanical problem that a piezoelectric actuator of thickness h, with the poling direction parallel to z-axis and an adhesive layer of thickness h', are bonded to a semi-infinite elastic structure, have been derived in terms of the interfacial shear and normal stresses τ and σ as

$$\begin{aligned}&\frac{2}{\pi\overline{E}^s}\int_{-c}^{-b}\frac{\tau(\xi)}{y-\xi}d\xi+\frac{2}{\pi\overline{E}^s}\int_{b}^{c}\frac{\tau(\xi)}{y-\xi}d\xi-(\frac{1-2\nu}{1-\nu})\frac{1}{\overline{E}^s}\sigma(y)\\&+\frac{1}{hE^p}\int_{b}^{y}\tau(y)dy-\frac{T}{hE^p}+\frac{e_{31}^pE_z}{E^p}=\frac{1}{k_1}\frac{d\tau}{dy},\end{aligned}\tag{4.1}$$

$$\begin{aligned}&\frac{2}{\pi\overline{E}^s}\int_{-c}^{-b}\frac{\sigma(\xi)}{y-\xi}d\xi+\frac{2}{\pi\overline{E}^s}\int_{b}^{c}\frac{\sigma(\xi)}{y-\xi}d\xi+(\frac{1-2\nu}{1-\nu})\frac{1}{\overline{E}^s}\tau(y)\\&-\frac{1}{E^pI}\int_{b}^{y}\int_{b}^{\zeta}\int_{b}^{\eta}\sigma(\xi)d\xi d\eta d\zeta+\frac{M_b(y-b)}{E^pI}+\frac{M_b}{E^pI}b=\frac{1}{k_2}\frac{d\sigma}{dy}.\end{aligned}\tag{4.2}$$

Also, the continuity of displacement at one end of the debonding point ($y = b$) will result in

$$\frac{2}{\pi \overline{E}^s}\left[\int_{-c}^{-b} \ln\left|\frac{b-\xi}{\xi}\right| \tau(\xi)d\xi + \int_{b}^{c} \ln\left|\frac{b-\xi}{\xi}\right| \tau(\xi)d\xi\right] + \frac{e_{31}^p E_z - T/h}{E^p} b = \frac{\tau(b)}{k_1}, \quad (4.3)$$

$$\theta_b - \frac{M_b}{E^p I} b = 0, \quad (4.4)$$

where T and M_b are the axial force, the bending moment of the piezoelectric actuator at the tips of the debonded part, and τ and σ are the interfacial normal and shear stresses, respectively. By making use of the boundary conditions of this model, the following relations can be obtained

$$\int_{-c}^{-b} \tau(\xi)d\xi = -T, \quad \int_{b}^{c} \tau(\xi)d\xi = T, \quad (4.5)$$

$$-\int_{b}^{c}\int_{b}^{y} \sigma(\xi)d\xi dy + M_b = 0, \quad (4.6)$$

and

$$\int_{b}^{c} \sigma(\xi)d\xi = 0, \quad (4.7)$$

in which equation (4.5) shows that the total interfacial shear force along the bonded part is equal to the compressive force T at the end of the debonded part ($y = -b$ or $y = b$); equation (4.6) illustrates that the double integral of the interfacial normal stress is equal to the bending moment at the right tip of the debonding part, as well-known for Euler-Bernoulli beam theory; equation (4.7) defines that the total interfacial normal force along the bonded part is equal to zero at the right tip of the debonding part. Here the governing equations, equations (4.1) - (4.7), can be solved numerically by using the Chebyshev polynomials. To

solve these equations, firstly, the following functions in equations (4.2) and (4.6) have been defined as

$$F(y) = \int_b^y \int_b^\zeta \int_b^\eta \sigma(\xi) d\xi d\eta d\zeta, \tag{4.8}$$

$$G(y) = \int_b^c \int_b^y \sigma(\xi) d\xi dy. \tag{4.9}$$

After a simple mathematical manipulation, equations (4.8) and (4.9) can be simplified as

$$F(y) = \frac{1}{2} \int_b^y (y-\xi)^2 \sigma(\xi) d\xi, \tag{4.10}$$

$$G(y) = \int_b^c (c-\xi)\sigma(\xi) d\xi. \tag{4.11}$$

Substituting equations (4.10) and (4.11) into equations (4.2) and (4.6) will yield, respectively,

$$\begin{aligned} &\frac{2}{\pi \overline{E}^s} \int_{-c}^{-b} \frac{\sigma(\xi)}{y-\xi} d\xi + \frac{2}{\pi \overline{E}^s} \int_b^c \frac{\sigma(\xi)}{y-\xi} d\xi + \left(\frac{1-2\nu}{1-\nu}\right) \frac{1}{\overline{E}^s} \tau(y) \\ &- \frac{1}{E^p I} \frac{1}{2} \int_b^y (y-\xi)^2 \sigma(\xi) d\xi + \frac{M_b(y-b)}{E^p I} - \theta_b = \frac{1}{k_2} \frac{d\sigma}{dy}, \end{aligned} \tag{4.12}$$

$$-\int_b^c (c-\xi)\sigma(\xi) d\xi + M_b = 0. \tag{4.13}$$

The singular integral equations, equations (4.1), (4.3), (4.5), (4.7), (4.12) and (4.13), can then be normalized to the non-dimensional forms as

$$\begin{aligned} &\int_{-c}^{-b} \frac{\tau^*(\xi)}{y-\xi} d\xi + \int_b^c \frac{\tau^*(\xi)}{y-\xi} d\xi - \left(\frac{1-2\nu}{1-\nu}\right) \frac{\pi}{2} \sigma^* \\ &+ \frac{\pi \overline{E^s}}{2} \frac{1}{hE^p} \int_b^y \tau^* dy - T^* - \frac{1}{k_1} \frac{\pi \overline{E}^s}{2} \frac{d\tau^*}{dy} = -1, \end{aligned} \tag{4.14}$$

$$\int_{-c}^{-b}\frac{\sigma^*(\xi)}{y-\xi}d\xi+\int_{b}^{c}\frac{\sigma^*(\xi)}{y-\xi}d\xi+(\frac{1-2\nu}{1-\nu})\frac{\pi}{\sigma_b}\tau^* \\ -\frac{1}{2E^pI}\frac{\pi\overline{E^s}}{2}\int_b^y(y-\xi)^2\sigma^*(\xi)d\xi+\frac{M_b(y-b)}{\sigma_bI}-\theta_b\frac{E^p}{\sigma_b}-\frac{1}{k_2}\frac{\pi\overline{E}^s}{2}\frac{d\sigma^*}{dy}=0, \tag{4.15}$$

$$\int_{-c}^{-b}\ln\left|\frac{b-\xi}{\xi}\right|\tau^*(\xi)d\xi+\int_b^c\ln\left|\frac{b-\xi}{\xi}\right|\tau^*(\xi)d\xi-T^*b-\frac{1}{k_1}\frac{\pi\overline{E}^s}{2}\tau^*(b)=-b, \tag{4.16}$$

$$\int_b^c\tau^*(\xi)d\xi=T/\left(\frac{\pi}{2}\frac{\overline{E^s}}{E^p}\sigma_b\right), \tag{4.17}$$

$$\int_b^c\sigma^*(\xi)\xi d\xi-M_b/\left(\frac{\pi}{2}\frac{\overline{E^s}}{E^p}\sigma_b\right)=0, \tag{4.18}$$

and

$$\int_b^c\sigma^*(\xi)d\xi=0. \tag{4.19}$$

The normalized shear stress, normal stress, and axial force are given by

$$\tau^*=\tau/p,\quad \sigma^*=\sigma/p,\quad T^*=\frac{T}{h\sigma_b}, \tag{4.20}$$

with

$$p=\frac{\pi e_{31}^pE_z\overline{E^s}}{2E^p}=\frac{\pi}{2}\frac{\overline{E^s}}{E^p}\sigma_b, \tag{4.21}$$

where $\sigma_b=e_{31}^pE_z$ is the blocking stress of the piezoelectric actuator.

The integral, $\int_b^y\tau^*dy$, in equation (4.14) can be rewritten as

$$\int_b^y\tau^*dy=-\int_y^c\tau^*dy+T/\left(\frac{\pi}{2}\frac{\overline{E^s}}{E^p}\sigma_b\right), \tag{4.22}$$

and the bending moment is normalized by

$$M_b^*=\frac{bM_b}{I\sigma_b}. \tag{4.23}$$

Finally, the singular integral equations can be rewritten as,

$$\int_{-c}^{-b}\frac{\tau^*(\xi)}{y-\xi}d\xi+\int_{b}^{c}\frac{\tau^*(\xi)}{y-\xi}d\xi-(\frac{1-2\nu}{1-\nu})\frac{\pi}{2}\sigma^*-\frac{\pi\overline{E^s}}{2}\frac{1}{hE^p}\int_{y}^{c}\tau^*dy-\frac{1}{k_1}\frac{\pi\overline{E}^s}{2}\frac{d\tau^*}{dy}=-1, \tag{4.24}$$

$$\begin{aligned}&\int_{-c}^{-b}\frac{\sigma^*(\xi)}{y-\xi}d\xi+\int_{b}^{c}\frac{\sigma^*(\xi)}{y-\xi}d\xi+(\frac{1-2\nu}{1-\nu})\frac{\pi}{\sigma_b}\tau^*-\frac{\pi\overline{E^s}}{4E^pI}\int_{b}^{y}(y-\xi)^2\sigma^*(\xi)d\xi\\&+M_b^*\left(\frac{y-b}{b}\right)-\theta_b^*-\frac{1}{k_2}\frac{\pi\overline{E}^s}{2}\frac{d\sigma^*}{dy}=0,\end{aligned} \tag{4.25}$$

$$\int_{-c}^{-b}\ln\left|\frac{b-\xi}{\xi}\right|\tau^*(\xi)d\xi+\int_{b}^{c}\ln\left|\frac{b-\xi}{\xi}\right|\tau^*(\xi)d\xi-T^*b-\frac{1}{k_1}\frac{\pi\overline{E}^s}{2}\tau^*(b)=-b, \tag{4.26}$$

$$\int_{b}^{c}\tau^*(\xi)d\xi=T^*\frac{2E^ph}{\pi\overline{E}^s}, \tag{4.27}$$

$$\int_{b}^{c}\sigma^*(\xi)d\xi=0, \tag{4.28}$$

and

$$\int_{b}^{c}\sigma^*(\xi)\xi d\xi-M_b^*\frac{2}{\pi}\frac{E^p}{\overline{E^s}}\frac{I}{b}=0. \tag{4.29}$$

Then, the axial force T, the bending moment M_b, the interfacial shear and normal stress τ and σ can be readily determined from the applied electric field.

Two local coordinates η_1 and η_2 normalized for the two bonded parts of the actuator are needed to get the solution. The origin of the first local coordinate η_1 is located at the center of the left bonded part of the actuator, and the origin of the second local coordinate η_2 is located at the center of the right bonded part of the actuator. Here, η_1 and η_2 are given by

$$\eta_1=\frac{\xi-d_1}{c_1},\quad \eta_2=\frac{\xi-d_2}{c_2}, \tag{4.30}$$

where

$$c_1 = c_2 = \left(\frac{c-b}{2}\right), \quad d_1 = -\left(\frac{b+c}{2}\right), \quad d_2 = \left(\frac{b+c}{2}\right). \tag{4.31}$$

In what follows, the left and right ends of two bonded parts of the actuator correspond to -1 and 1 in the local coordinates, respectively. The integrals in the equations above, which are related to the interfacial shear stress, can be changed to

$$\int_{-c}^{-b} \frac{\tau_1^*(\xi)}{y-\xi} d\xi = \int_{-1}^{1} \frac{\tau_1^*}{y_1-\eta_1} d\eta_1, \tag{4.32}$$

$$\int_{b}^{c} \frac{\tau_2^*(\xi)}{y-\xi} d\xi = \int_{-1}^{1} \frac{\tau_2^*}{y_2-\eta_2} d\eta_2, \tag{4.33}$$

$$\int_{y}^{c} \tau_2^*(\xi) dy = c_2 \int_{y_2}^{1} \tau_2^* d\eta_2, \tag{4.34}$$

$$\int_{-c}^{-b} \ln\left|\frac{b-\xi}{\xi}\right| \tau_1^*(\xi) d\xi = \frac{c_1}{2} \int_{1}^{2\frac{\alpha_0}{\alpha_1}-2\frac{\alpha_2}{\alpha_1}-1} \int_{-1}^{1} \frac{\tau_1^* d\eta_1}{y_1-\eta_1} d\eta_1, \tag{4.35}$$

$$\int_{b}^{c} \ln\left|\frac{b-\xi}{\xi}\right| \tau_2^*(\xi) d\xi = \frac{c_2}{2} \int_{-2\frac{\alpha_0}{\alpha_2}+2\frac{\alpha_1}{\alpha_2}+1}^{-1} \int_{-1}^{1} \frac{\tau_2^* d\eta_2}{y_2-\eta_2} d\eta_2, \tag{4.36}$$

with

$$\alpha_0 = \frac{c}{h}, \qquad \alpha_1 = \frac{c_1}{h}, \qquad \alpha_2 = \frac{c_2}{h}. \tag{4.37}$$

And the integrals related to the interfacial normal stress can be similarly reorganized as

$$\int_{-c}^{-b} \frac{\sigma_1^*(\xi)}{y-\xi} d\xi = \int_{-1}^{1} \frac{\sigma_1^*}{y_1-\eta_1} d\eta_1, \tag{4.38}$$

$$\int_{b}^{c} \frac{\sigma_2^*(\xi)}{y-\xi} d\xi = \int_{-1}^{1} \frac{\sigma_2^*}{y_2-\eta_2} d\eta_2, \tag{4.39}$$

$$\int_b^c \sigma_2^*(\xi)\xi d\xi = c_2 d_2 \int_{-1}^1 \sigma_2^* d\eta_2 + c_2^2 \int_{-1}^1 \sigma_2^* \eta_2 d\eta_2, \tag{4.40}$$

$$\int_b^y (y-\xi)^2 \sigma_2^*(\xi) dy = c_2^3 \int_{-1}^{y_2} (y_2-\eta_2)^2 \sigma_2^* d\eta_2. \tag{4.41}$$

Then, the integral equations (4.24)-(4.29), can be further rewritten as

$$\begin{aligned} &\int_{-1}^1 \frac{\tau_1^*}{y_1-\eta_1} d\eta_1 + \int_{-1}^1 \frac{\tau_2^*}{y_2-\eta_2} d\eta_2 - (\frac{1-2\nu}{1-\nu})\frac{\pi}{2}\sigma^* \\ &- \frac{\pi\overline{E^s}}{2}\frac{1}{hE^p}c_2 \int_{y_2}^1 \tau_2^* d\eta_2 - \frac{1}{k_1}\frac{\pi\overline{E}^s}{2}\frac{d\tau^*}{dy} = -1, \end{aligned} \tag{4.42}$$

$$\begin{aligned} &\int_{-1}^1 \frac{\sigma_1^*}{y_1-\eta_1} d\eta_1 + \int_{-1}^1 \frac{\sigma_2^*}{y_2-\eta_2} d\eta_2 + (\frac{1-2\nu}{1-\nu})\frac{\pi}{2}\tau^* - \frac{\pi\overline{E^s}}{4E^p I}c_2^3 \int_{-1}^{y_2} (y_2-\eta_2)^2 \sigma_2^* d\eta_2 \\ &+ M_b^*(y_2+1)\left(\frac{c_2}{b}\right) - \theta_b^* - \frac{1}{k_2}\frac{\pi\overline{E}^s}{2}\frac{d\sigma^*}{dy} = 0, \end{aligned} \tag{4.43}$$

$$\begin{aligned} &\frac{c_1}{2}\int_1^{2\frac{\alpha_0}{\alpha_1}-2\frac{\alpha_2}{\alpha_1}-1} \int_{-1}^1 \frac{\tau_1^* d\eta_1}{y_1-\eta_1} d\eta_1 + \frac{c_2}{2}\int_{-2\frac{\alpha_0}{\alpha_2}+2\frac{\alpha_1}{\alpha_2}+1}^{-1} \int_{-1}^1 \frac{\tau_2^* d\eta_2}{y_2-\eta_2} d\eta_2 \\ &- T^* b - \frac{1}{k_1}\frac{\pi\overline{E}^s}{2}\tau^*(b) = -b, \end{aligned} \tag{4.44}$$

$$c_2 \int_{-1}^1 \tau_2^* d\eta_2 = T \Big/ \left(\frac{\pi}{2}\frac{\overline{E^s}}{E^p}\sigma_b\right), \tag{4.45}$$

$$c_2 \int_{-1}^1 \sigma_2^* d\eta_2 = 0, \tag{4.46}$$

and

$$c_2 d_2 \int_{-1}^1 \sigma_2^* d\eta_2 + c_2^2 \int_{-1}^1 \sigma_2^* \eta_2 d\eta_2 - M_b^* \frac{2}{\pi}\frac{E^p}{\overline{E^s}}\frac{I}{b} = 0. \tag{4.47}$$

4.3 General solutions using Chebyshev polynomial expansion

Because the resulting governing equations (4.42)-(4.47) are singular integral equations, the solutions involve a square-root singularity at the ends of the bonded parts (Muskhelishvili, 1953). Accordingly, the general solutions of interfacial shear and normal stresses can be expressed in terms of the following expansion of Chebyshev polynomials of the first kind as

$$\tau_1^* = \frac{d_0^{(1)}}{(1-\eta_1^2)^{1/2}} + \frac{1}{(1-\eta_1^2)^{1/2}} \sum_{i=1}^{\infty} d_i^{(1)} T_i(\eta_1), \tag{4.48}$$

$$\tau_2^* = \frac{d_0^{(2)}}{(1-\eta_2^2)^{1/2}} + \frac{1}{(1-\eta_2^2)^{1/2}} \sum_{i=1}^{\infty} d_i^{(2)} T_i(\eta_2), \tag{4.49}$$

$$\sigma_1^* = \frac{e_0^{(1)}}{(1-\eta_1^2)^{1/2}} + \frac{1}{(1-\eta_1^1)^{1/2}} \sum_{i=1}^{\infty} e_i^{(1)} T_i(\eta_1), \tag{4.50}$$

$$\sigma_2^* = \frac{e_0^{(2)}}{(1-\eta_2^2)^{1/2}} + \frac{1}{(1-\eta_2^2)^{1/2}} \sum_{i=1}^{\infty} e_i^{(2)} T_i(\eta_2), \tag{4.51}$$

where T_i is the Chebyshev polynomial of the first kind. It is defined by the relation $T_i(\eta) = \cos i\theta$ when $\eta = \cos\theta$.

For the current problem, the interfacial shear and normal stresses along the bonded part of the actuator satisfy the symmetric relation that

$$\tau_1^*(\eta_1) = -\tau_2^*(-\eta_1), \quad \sigma_1^*(\eta_1) = \sigma_2^*(-\eta_1). \tag{4.52}$$

Substituting equations (4.48)-(4.51) into equation (4.52), the following recursive relations

for the right part and left part of the actuator can be derived,

$$d_0^{(1)} = -d_0^{(2)}, \quad d_1^{(1)} = d_1^{(2)}, \quad d_2^{(1)} = -d_2^{(2)}, \quad \ldots \quad d_i^{(1)} = (-1)^{i+1} d_i^{(2)}, \tag{4.53}$$

$$e_0^{(1)} = e_0^{(2)}, \quad e_1^{(1)} = -e_1^{(2)}, \quad e_2^{(1)} = e_2^{(2)}, \quad \ldots \quad e_i^{(1)} = (-1)^{i} e_i^{(2)}. \tag{4.54}$$

In the following discussion, only the right bonded part is considered. Here, the Chebyshev polynomial expansions are truncated to the $(N-2)^{th}$ term. The equations are satisfied at the following collocation points at each bonded segment of the actuator, given by

$$\eta_j = \cos\frac{j-1}{N-1}\pi, \quad j = 2,3,\ldots,N-1. \tag{4.55}$$

Through the Chebyshev polynomial expansion, the first part of equation (4.42) becomes

$$\int_{-1}^{1} \frac{\tau_1^*}{y_1 - \eta_1} d\eta_1 = -\pi \sum_{i=1}^{N-2} d_i^{(2)} \left[\sqrt{(y_{1j}^*)^2 - 1} - y_{1j}^*\right]^i \frac{(-1)^i}{\sqrt{(y_{1j}^*)^2 - 1}} - \pi d_0^{(2)} / \sqrt{(y_{1j}^*)^2 - 1}, \tag{4.56}$$

where

$$y_{1j}^* = \eta_j + 2\frac{c+b}{c-b}, \tag{4.57}$$

which is the coordinate of collocation point j in the left bonded part of the actuator.

The second part of equation (4.42) becomes

$$\int_{-1}^{1} \frac{\tau_2^*}{y_2 - \eta_2} d\eta_2 = -\pi \sum_{i=1}^{N-2} d_i^{(2)} \frac{\sin\left[i\frac{j-1}{N-1}\pi\right]}{\sin\left[\frac{j-1}{N-1}\pi\right]}. \tag{4.58}$$

The third part of equation (4.42) becomes

$$\left(\frac{1-2\nu}{1-\nu}\right)\frac{\pi}{2}\sigma^* = \left(\frac{1-2\nu}{1-\nu}\right)\frac{\pi}{2} \sum_{i=1}^{N-2} e_i^{(2)} \frac{\cos\left[i\frac{j-1}{N-1}\pi\right]}{\sin\left[\frac{j-1}{N-1}\pi\right]}. \tag{4.59}$$

The fourth part of equation (4.42) becomes

$$\frac{\pi\overline{E^s}}{2}\frac{1}{hE^p}c_2\int_{y_2}^{1}\tau_2^* d\eta_2 = \pi\sum_{i=1}^{N-2} d_i^{(2)}\sin\left[i\frac{j-1}{N-1}\pi\right]\frac{\lambda\alpha_2}{\pi i} - \lambda\alpha_2\pi\frac{j-1}{N-1}d_0^{(2)}, \tag{4.60}$$

where

$$\lambda = \frac{\pi\overline{E}^s}{2E^p}. \tag{4.61}$$

The last part of equation (4.42) becomes

$$\frac{d\tau^*}{dy} = \frac{1}{c_2}\sum_{i=0}^{N-2} d_i^{(2)}\left\{\frac{\cos\left[i\frac{j-1}{N-1}\pi\right]\cos\left[\frac{j-1}{N-1}\pi\right]}{\left(\sin\left[\frac{j-1}{N-1}\pi\right]\right)^3} + i\frac{\sin\left[i\frac{j-1}{N-1}\pi\right]}{\left(\sin\left[\frac{j-1}{N-1}\pi\right]\right)^2}\right\} \tag{4.62}$$

Combined with equation (4.53), equation (4.42) reduces to

$$\begin{aligned}
&-\pi\sum_{i=1}^{N-2} d_i^{(2)}\left\{\frac{\sin\left[i\frac{j-1}{N-1}\pi\right]}{\sin\left[\frac{j-1}{N-1}\pi\right]} + \left[\sqrt{(y_{1j}^*)^2-1}-y_{1j}^*\right]^i/\sqrt{(y_{1j}^*)^2-1}\right\}\\
&-\pi\sum_{i=1}^{N-2} d_i^{(2)}\sin\left[i\frac{j-1}{N-1}\pi\right]\frac{\lambda\alpha_2}{\pi i} - \lambda\alpha_2\pi\frac{j-1}{N-1}d_0^{(2)} - \pi d_0^{(2)}/\sqrt{(y_{1j}^*)^2-1}\\
&-\left(\frac{1-2\nu}{1-\nu}\right)\frac{\pi}{2}\sum_{i=1}^{N-2} e_i^{(2)}\frac{\cos\left[i\frac{j-1}{N-1}\pi\right]}{\sin\left[\frac{j-1}{N-1}\pi\right]} - \frac{1}{k_1}\frac{\pi\overline{E}^s}{2}\frac{d\tau^*}{dy} = -1, \quad j = 2,3,...,N-1.
\end{aligned} \tag{4.63}$$

Similarly, the equations (4.43) and (4.44) lead to

$$\begin{aligned}
&-\pi\sum_{i=1}^{N-2} e_i^{(2)}\left\{\frac{\sin\left[i\frac{j-1}{N-1}\pi\right]}{\sin\left[\frac{j-1}{N-1}\pi\right]} - \left[\sqrt{(y_{1j}^*)^2-1}-y_{1j}^*\right]^i/\sqrt{(y_{1j}^*)^2-1}\right\}\\
&+\left(\frac{1-2\nu}{1-\nu}\right)\frac{\pi}{2}\sum_{i=1}^{N-2} d_i^{(2)}\frac{\cos\left[i\frac{j-1}{N-1}\pi\right]}{\sin\left[\frac{j-1}{N-1}\pi\right]} - \frac{\pi\overline{E^s}}{4E^pI}c_2^3\sum_{i=1}^{N-2} e_i^{(2)}\int_{-1}^{\eta_j}(\eta_j-\xi)^2\frac{T_i(\xi)}{\sqrt{1-\xi^2}}(\xi)d\xi\\
&+M_b^*(\eta_j+1)\frac{c_2}{b} - \theta_b^* - \frac{1}{k_2}\frac{\pi\overline{E}^s}{2}\frac{d\sigma^*}{dy} = 0, \quad j = 2,3,...,N-1,
\end{aligned} \tag{4.64}$$

$$-\pi\frac{c_2}{2}\sum_{i=1}^{N-2} d_i^{(2)}\left[\int_1^{2\frac{\alpha_0}{\alpha_1}-2\frac{\alpha_2}{\alpha_1}-1}\frac{\left[\sqrt{(y_1)^2-1}-y_1\right]^i}{\sqrt{(y_1)^2-1}}dy_1+\int_{-2\frac{\alpha_0}{\alpha_2}+2\frac{\alpha_1}{\alpha_2}+1}^{-1}\frac{\left[\sqrt{(y_2)^2-1}-y_2\right]^i}{\sqrt{(y_2)^2-1}}dy_2\right]$$
$$-\pi\frac{c_2}{2}d_0^{(2)}\left[\int_1^{2\frac{\alpha_0}{\alpha_1}-2\frac{\alpha_2}{\alpha_1}-1}\frac{1}{\sqrt{(y_1)^2-1}}dy_1+\int_{-2\frac{\alpha_0}{\alpha_2}+2\frac{\alpha_1}{\alpha_2}+1}^{-1}\frac{1}{\sqrt{(y_2)^2-1}}dy_2\right]$$
$$-T^*b-\frac{1}{k_1}\frac{\pi\overline{E}^s}{2}\tau^*(b)=-b. \tag{4.65}$$

Substituting equations (4.49) and (4.51) into equations (4.45) - (4.47) and making use of the orthogonality of Chebyshev polynomials referred from Appendix A.2, the unknown coefficients $d_0^{(2)}$, $e_0^{(2)}$ and $e_1^{(2)}$ can be readily determined. Here, $d_0^{(2)}$ is expressed in terms of the axial force in the debonded part; $e_0^{(2)}$ and $e_1^{(2)}$ are related to the bending moment at the tips of the debonded part, i.e.,

$$d_0^{(2)}=\frac{E^pI}{\pi pc_2}\alpha^2, \tag{4.66}$$

$$e_0^{(2)}=0, \tag{4.67}$$

$$e_1^{(2)}=-(\frac{2}{\pi})^2\frac{E^p}{\overline{E^s}}\frac{I}{c_2b^2}M_b^*, \tag{4.68}$$

with $\alpha^2=T^*h\sigma_b/E^pI$.

The algebraic equations (4.63), (4.64) and (4.65) contain $(N-1)$ unknowns for $d_i^{(2)}, i=0,1,2,...N-2$, $(N-3)$ unknowns for $e_i^{(2)}, i=2,...N-2$ and M_b^*. These $2N-3$ unknowns can be solved through $(2N-3)$ equations, corresponding to $(N-2)$ equations from (4.63), $(N-2)$ equations from (4.64) and one equation from (4.65).

Chapter 5: Results and Discussion

The solution obtained in the previous chapter can be used to evaluate the distribution of the resultant stresses and forces. In this chapter, the FEM simulation is conducted to verify the current model at first. Then, in order to evaluate the effects of different material properties, the geometries of the piezoelectric actuator model components and the interfacial debonding of the current model on the electromechanical behavior of the integrated actuator-host structure are presented. The attention is focused on the distributions of the shear stress, normal stress, axial force, bending moment and axial displacement along the interface between the adhesive layer and host structure. The convergence of the solution by using Chebyshev polynomial expansion is carefully evaluated, which uses 40 terms to ensure the current results considered convergent.

5.1 Comparison with FEM results

To verify the validity of the current model with bending and adhesive layer, the finite element method is also implemented to determine stress distribution along the adhesive layer. The COMSOL Multiphysics 5.2a is chosen for modelling the piezoelectric actuator system. A static analysis of the model with a piezoelectric actuator attached to a semi-infinite host through a thin adhesive layer between them has been conducted. Here, a PZT ceramic as the piezoelectric material and aluminum as the elastic material are chosen for analytical calculations and numerical simulations. The piezoelectric actuator material (PZT-4) with poling along z direction is a transversely isotropic material; the host is an isotropic material,

which is stiffer than the adhesive layer. Usually, the thickness of a typical thin piezoelectric ceramic sheet is from 0.1mm to 1mm. So in the FEM model, the 0.1mm and 0.01mm are selected as the thickness of the piezoelectric actuator and adhesive layer, respectively. The length of the actuator and adhesive layer are 2mm. The length and thickness of the host are 10 times compared to the actuator in order to model the semi-infinite host structure. An electric field is applied along to the poling direction of the actuator. In the numerical model, mapped square elements and free triangular elements are utilized for the piezoelectric actuator and adhesive layer and the host structure, respectively. Specifically, the quad element size in the piezoelectric actuator is around $1.0 \times 10^{-2}h$ and there are at least 5 layers of elements in the adhesive layer to ensure the accuracy of the numerical simulation results. The mesh of FEM model for $h'/h = 10$ is shown in figure 5.1.

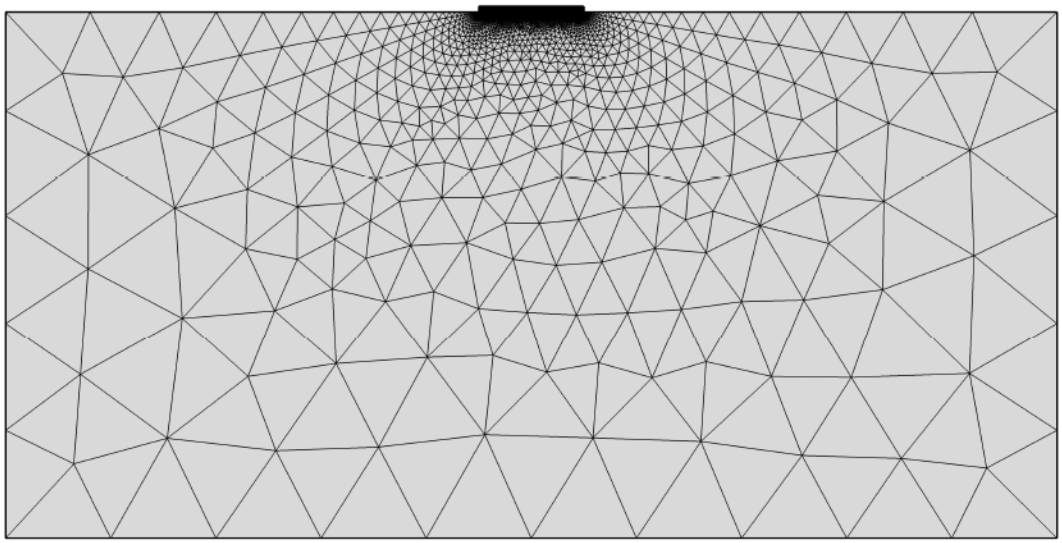

Figure 5.1: The mesh of the FEM model for $h'/h = 10$.

The elastic and piezoelectric constants of the piezoelectric actuator, host structure and adhesive layer are listed in Tables 5.1 and 5.2, respectively. All parameters are defined in

the appendix A.1.

Table 5.1: Material properties of the piezoelectric actuator

Elastic stiffness parameters	c_{11}	c_{12}	c_{13}	c_{33}	c_{44}
$(\times 10^{10} Pa)$	13.9	6.78	7.43	11.5	2.56
Piezoelectric constants	e_{31}	e_{33}	e_{15}		
(c/m^2)	-5.2	15.08	12.71		
Dielectric constants	ε_{11}	ε_{33}			
$(\times 10^{-9} C/Vm)$	6.45	5.62			

Table 5.2: Material properties of the host structure and adhesive layer

Host structure			
Young's modulus $E^s(\times 10^{10} Pa)$	5.27	Possion's ratio ν^s	0.3
Adhesive layer			
Young's modulus $E^a(\times 10^{9} Pa)$	2.6	Possion's ratio ν^a	0.3

Figure 5.2 shows the interfacial stress distribution no bending, with bending and FEM simulation with perfect bonding condition for $\lambda = 1$, $c/h = 10$ and $h'/c = 0.001$, which means there is an adhesive layer added to the system. The shear stress distribution is anti-symmetrical, and the normal stress distribution is symmetrical with regard to the center of piezoelectric actuator, respectively. It can be observed in figure 5.2 that a limited discrepancy exists near the ends of the piezoelectric actuator for normal stresses. Overall, the comparison shows a very good agreement between the current and FEM results. The error between current and FEM results are within 10% in the range of 0.5 to 0.85. The interfacial stresses with bending and FEM simulation results with the partially debonded actuator are shown in figure 5.3, for $\lambda = 1$, $c/h = 10$, $b/c = 0.5$ and $h'/c = 0.001$. Similar to the previous case with perfect bonding condition, shear stress with bending shows a good consistency with FEM simulation results. As shown in the governing equations (4.42) - (4.47)

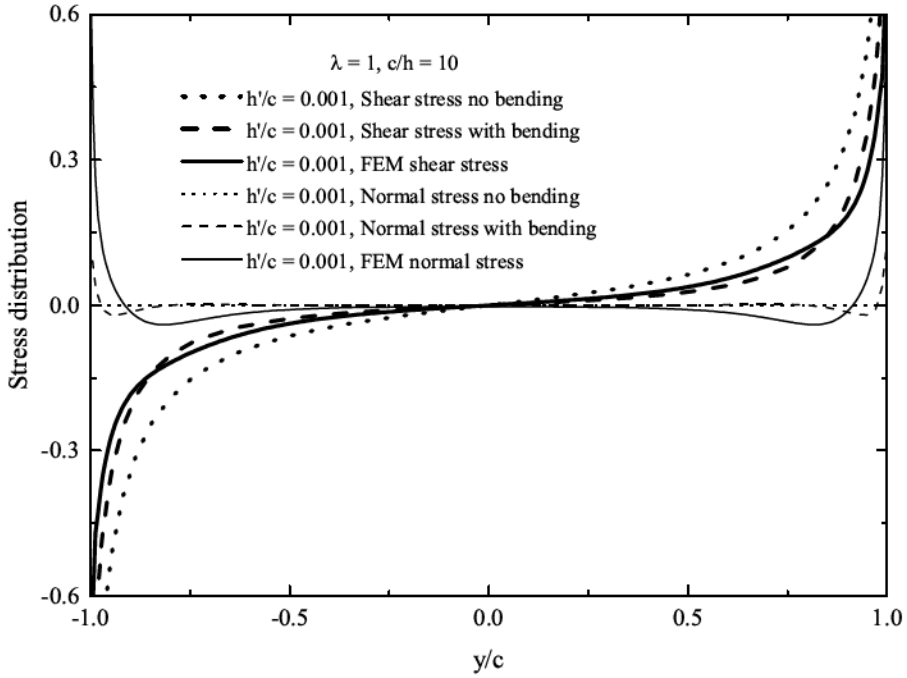

Figure 5.2: Interfacial stress distribution for the perfect bonding condition ($\lambda = 1, c/h = 10$ and $h^{'}/c = 0.001$).

of the piezoelectric system, the normalized interfacial stress, axial force, bending moment and axial displacement are controlled by these parameters, λ, c/h, h'/c and b/c. Here, λ represents material mismatch of the piezoelectric actuator and the host structure. c/h and h'/c illustrate the geometrical relation of the actuator and the adhesive layer, respectively. b/c represents the ratio of the debonding length and length of the piezoelectric actuator. As aforementioned, the thickness of a typical thin piezoelectric ceramic sheet is usually from 0.1 mm to 1 mm. If half of the length of the piezoelectric actuator is assumed to be 5 mm, the c/h would be in the range from 5 to 50. In the following discussion, the values of above parameters will vary to evaluate different electromechanical responses of the piezoelectric actuator system.

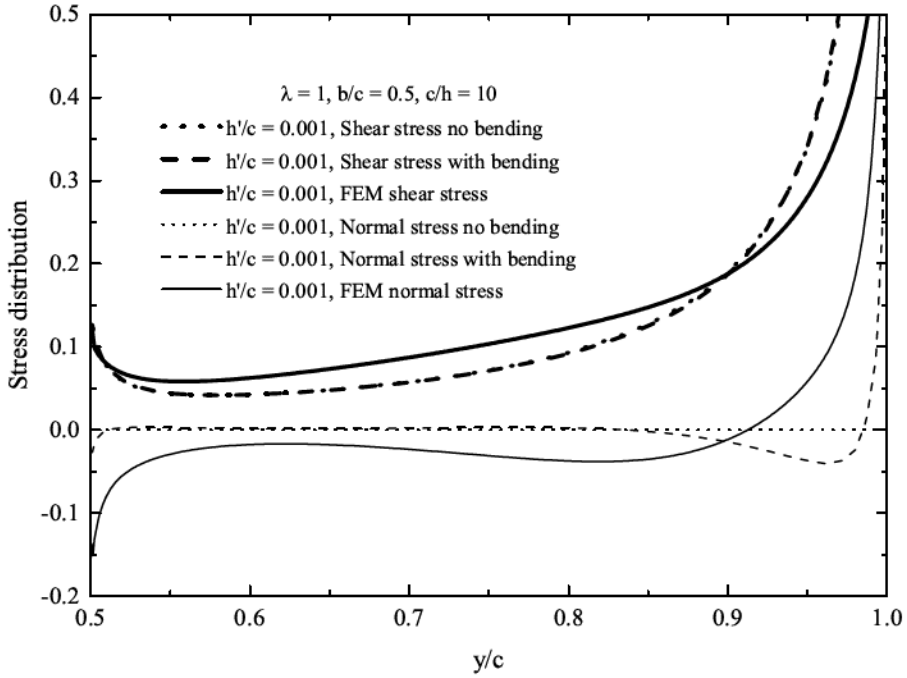

Figure 5.3: Interfacial stress distribution for the partial debonding condition ($\lambda = 1$, $b/c = 0.5$, $c/h = 10$ and $h^{'}/c = 0.001$).

5.2 The case for the piezoelectric actuator perfectly bonded to the semi-infinite elastic host with an adhesive layer

The variation of the interfacial shear and normal stresses with different h'/c for $\lambda = 1$ and $c/h = 10$ are shown in figures 5.4 and 5.5, respectively. The results of shear and normal stresses with bending match the FEM simulation results well. In these four scenarios, the highest stress concentration occurs at the ends of the piezoelectric actuator when $h'/c = 0$.

To study the effect of the material mismatch λ, the geometry of piezoelectric actuator is fixed. Figures 5.6 and 5.7 show the results for normalized interfacial stresses along the bonding interface for different λ with $h'/c = 0$ and 0.01, respectively. In these two figures,

both shear stress and normal stress along the interface show strong stress concentration at the ends of the piezoelectric actuator. In this case, a smaller λ means a stiffer piezoelectric actuator layer compared to the host structure and larger stress level at the ends of the

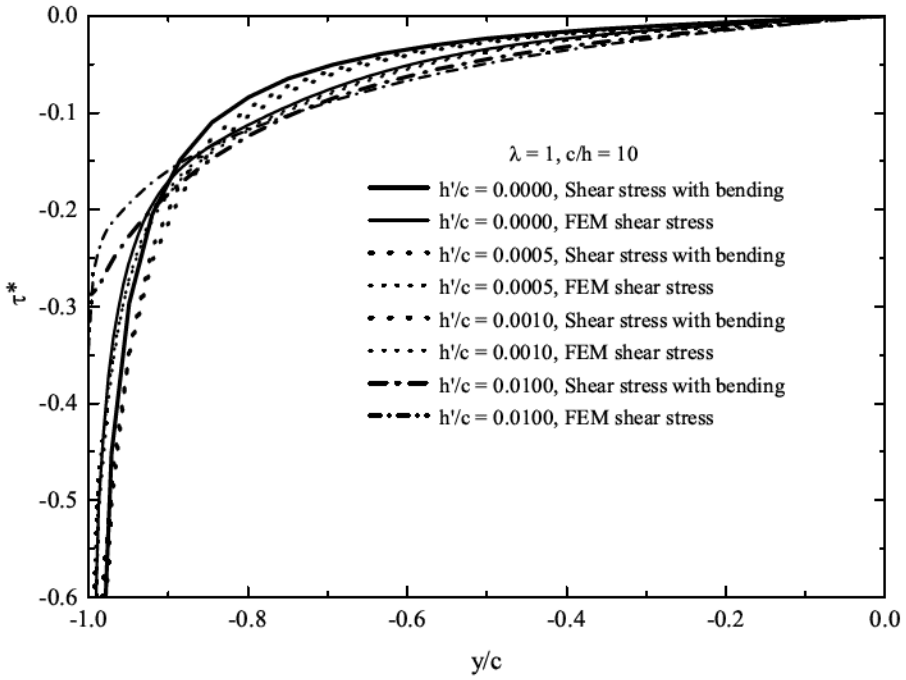

Figure 5.4: Interfacial shear stress distribution for the perfect bonding condition ($\lambda = 1$ and $c/h = 10$).

piezoelectric actuator. The stress concentration is more focused around the ends of the piezoelectric actuator with the larger value of the λ. The increased shear and normal stress level along the entire length of the actuator due to decreasing λ value are observed. 5.7 show that the stress level decreases with the adhesive layer involved, and the stress distribution becomes less concentrated around the ends of the piezoelectric actuator. Higher stress concentration indicates higher possibility of the debonding between the piezoelectric actuator and the host structure.

To investigate the effect of the geometry of the piezoelectric actuator, various ratios of

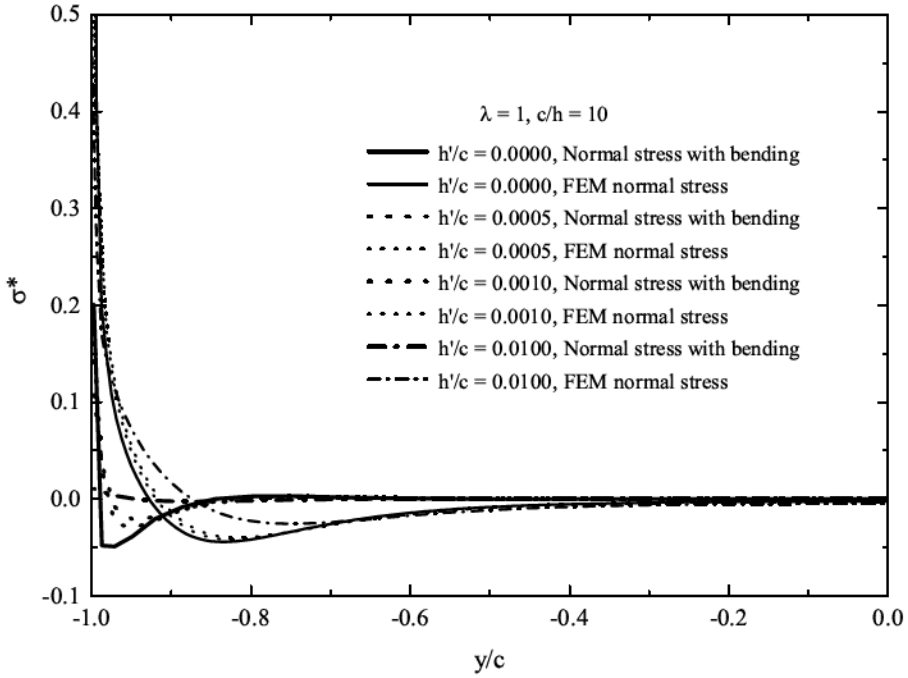

Figure 5.5: Interfacial normal stress distribution for the perfect bonding condition ($\lambda = 1$ and $c/h = 10$).

length to thickness, c/h, with the same material properties are considered. Specifically, $c/h = 5$, 10, 20, and 50 are chosen for two cases, $h'/c = 0$ and $h'/c = 0.01$, the stress distribution of which has been illustrated in figures 5.8 and 5.9, respectively. For the case without the adhesive layer, $h'/c = 0$, the stress distribution becomes more concentrated around the ends of the piezoelectric actuator with the increase of c/h, as shown in figure 5.8. With the increasing of c/h, an decreasing of interfacial stress level along the actuator can be observed. After adding the adhesive layer with $h'/c = 0.01$, the stress concentration decreases dramatically around the ends of the piezoelectric actuator, which can be clearly observed from figures 5.8 and 5.9.

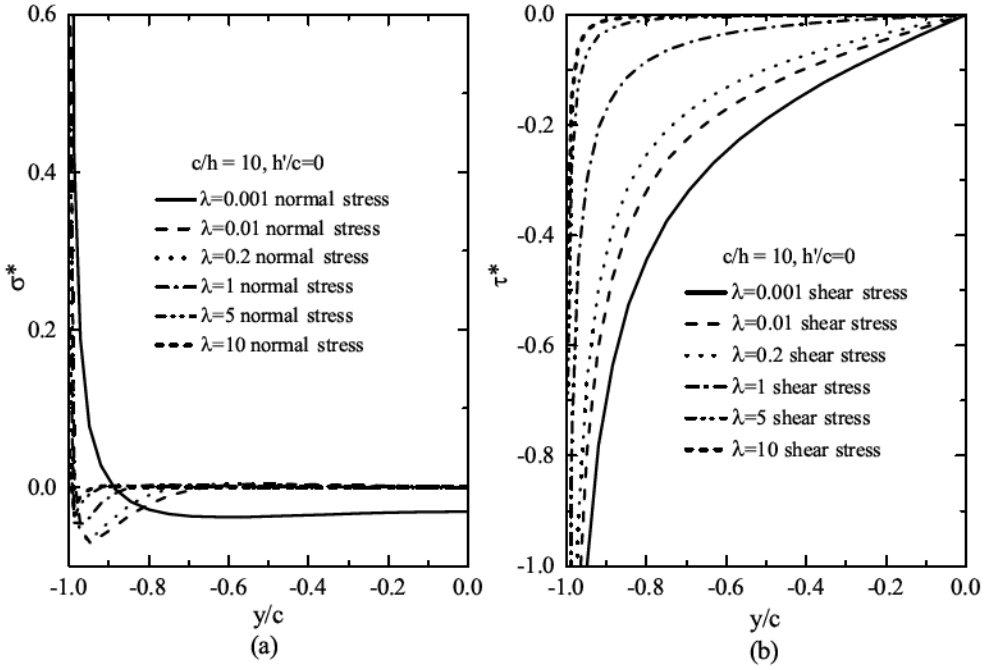

Figure 5.6: Interfacial stress distribution of current model for perfect bonding condition ($c/h = 10$ and $h^{'}/c = 0$).

5.3 The case for the piezoelectric actuator partially debonded to the semi-infinite elastic host with an adhesive layer

Debonding might occur due to poor bonding condition of high interface stress level around the piezoelectric actuator. The piezoelectric actuator is assumed to be debonded at the centre symmetrically, as shown in figure 3.3, where $2b$ represents the length of the debonding length. In the following section, half of the actuator will be discussed. After debonding occurs, the local stress distribution along the interface may change dramatically. The effect of the debonding length $2b$ on the redistribution of shear and normal stresses along the piezoelectric actuator for $\lambda = 1$ and $c/h = 20$ with $h^{'}/c = 0$ and $h^{'}/c = 0.01$ are shown in figures 5.10 and 5.11, where the results of the perfect bonding case is given for comparison.

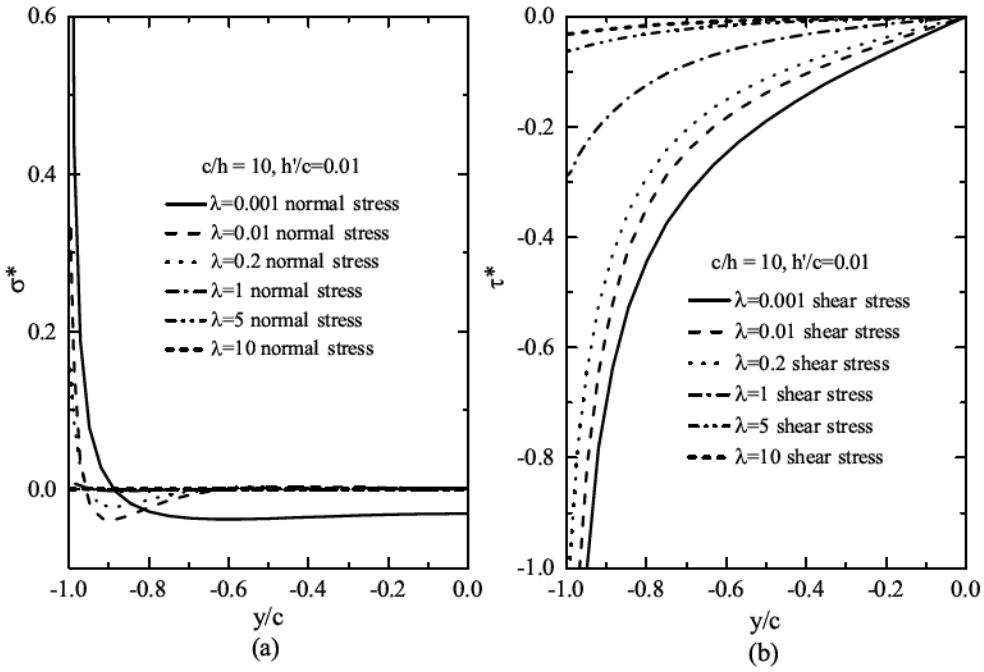

Figure 5.7: Interfacial stress distribution of current model for perfect bonding condition ($c/h = 10$ and $h^{'}/c = 0.01$).

It is obvious that the interfacial shear stress and normal stress vary significantly with different debonding length. The results show that the debonding causes stress concentration around the tip of the debonding part. It does not significantly affect the stress distribution far away from the debonding part. The stress concentration is increased at the two tips of the debonding part with the increase of the debonding length. However, when the adhesive layer is involved, the stress concentration near the debonding tip is decreased significantly, which can be observed in figures 5.10 and 5.11. Also, as shown in figure 5.11, the normal stress distribution, compared with that of the shear stress, is less affected by the debonding length.

Figures 5.12 and 5.13 illustrates the stress distribution variation along the piezoelectric actuator with central debondings for $\lambda = 1$, $b/c = 0.5$ with different c/h ratios for $h^{'}/c = 0$

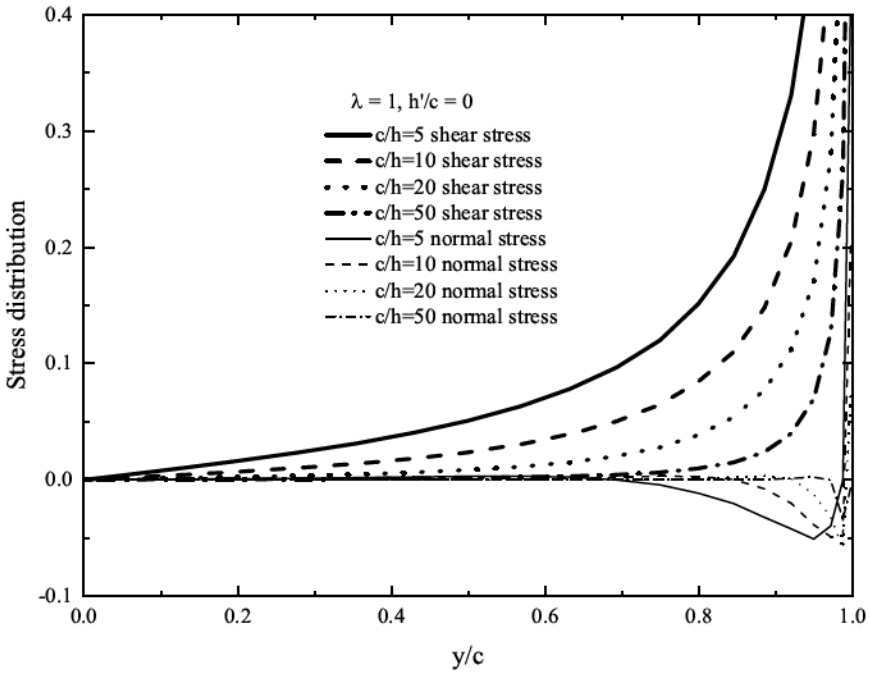

Figure 5.8: Interfacial stress distribution of current model for perfect bonding condition ($\lambda = 1$ and $h'/c = 0$).

and $h'/c = 0.01$, respectively. The results show that with the increase of c/h ratio, the interfacial stress levels along the piezoelectric actuator decrease, and the stress concentration at the tips of the debonding part decreases. As shown in figure 5.13, the stress concentration around the ends of the piezoelectric actuator is decreased significantly after an adhesive layer is included.

When debonding occurs, there is no stress transfer in the debonding part. However, the bending moment, axial force, and axial displacement at the debonding edge will affect the electromechanical behavior of the piezoelectric system. In the following discussion, the effects of these parameters will be investigated for different debonding lengths. Five different adhesive layer thicknesses ($h'/c = 0.000$, 0.001, 0.005, 0.010 and 0.020) for $\lambda = 1$ and $c/h = 20$ are studied. The normalized axial force $T^* = T/h\sigma_b$ in the debonded

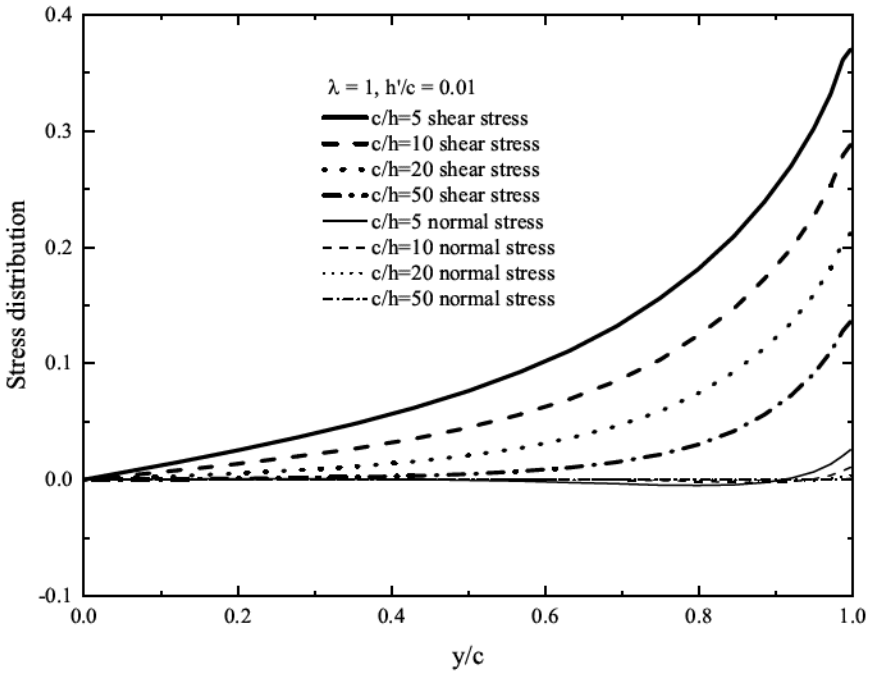

Figure 5.9: Interfacial stress distribution of current model for perfect bonding condition ($\lambda = 1$ and $h^{'}/c = 0.01$).

tip of the piezoelectric actuator, as a function of b/c with bending or without bending conditions, is shown in figure 5.14. There is no significant difference of the axial force at the ends of the piezoelectric actuator, indicating limited influence from the bending effect. It is, however, evident that the adhesive layer thickness has a significant effect upon the axial force. With the increase of adhesive layer thickness, the axial force decreases. From the figure 5.15, with the increase of λ, the axial force level is substantially increased. It should be mentioned that the normalized axial force varies very subtly when the debonding length is small for a given constant λ. Also, the normalized axial force is less sensitive to the change of the debonding length for larger λ, corresponding to a softer piezoelectric actuator. The normalized axial force tend to one when the actuator is extremely soft, which means the remaining actuator acts as a fixed boundary.

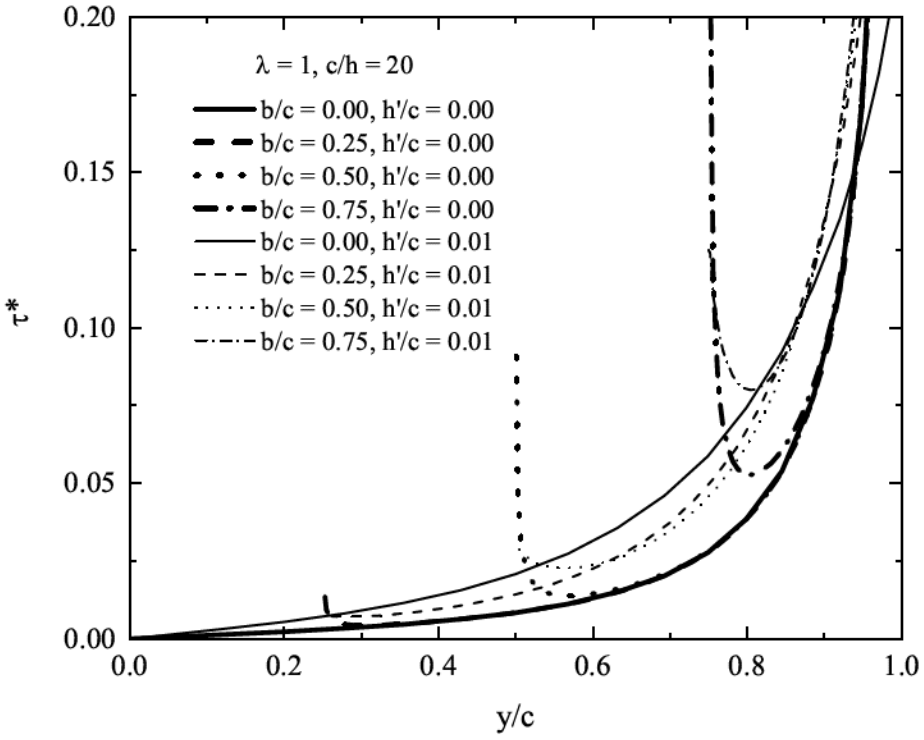

Figure 5.10: Shear stress distribution of current model for partial debonding actuators ($\lambda = 1$ and $c/h = 20$).

The variation of the normalized bending moment $M^* = bM_b/I\sigma_b$ in the debonded tip of the piezoelectric actuator with the normalized debonding length b/c is illustrated in figure 5.16. It shows that the bending moment increases with an increasing of the adhesive layer thickness. Figure 5.17 shows the variation of M^* with the debonding length for different material mismatch λ. The significance of the bending moment remarkably depends on the normalized debonding length. It is small when the normalized debonding length is short and increases rapidly when the normalized debonding length is over 0.7 . It is observed that M^* increases with decreasing λ. As expected, the bending moment is less sensitive to the normalized debonding length for a softer piezoelectric actuator.

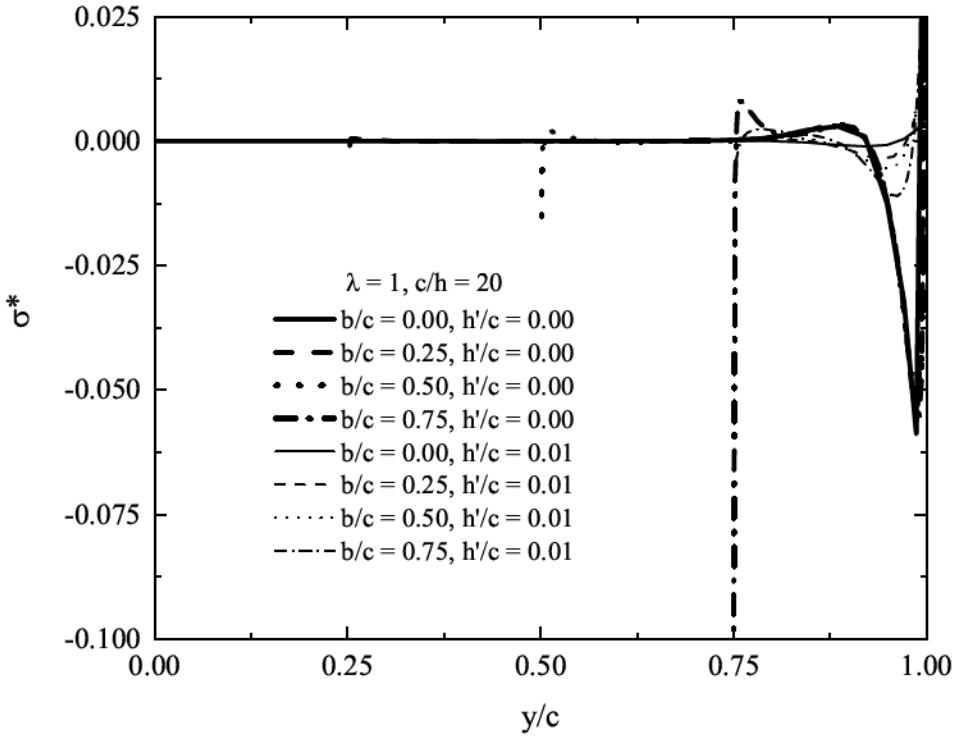

Figure 5.11: Normal stress distribution of current model for partial debonding actuators ($\lambda = 1$ and $c/h = 20$).

Figure 5.18 shows the normalized axial displacement $u^* = -\frac{b\sigma_b(T^*-1)}{E^p}$ at the debonded tip of the piezoelectric actuator with bending or without bending effects. It shows that the axial displacement with bending is almost the same as the displacement without bending, which can be expected from the result of axial force T^*. The bending effect doesn't have significant effect on the axial displacement at the debonded tip of the piezoelectric actuator. It can be observed that with the increase of the adhesive layer thickness or the normalized debonding length, the normalized axial displacement increases. The normalized axial displacement at the debonded tip of the piezoelectric actuator for five different material mismatch λ is shown in figure 5.19. When the piezoelectric actuator becomes

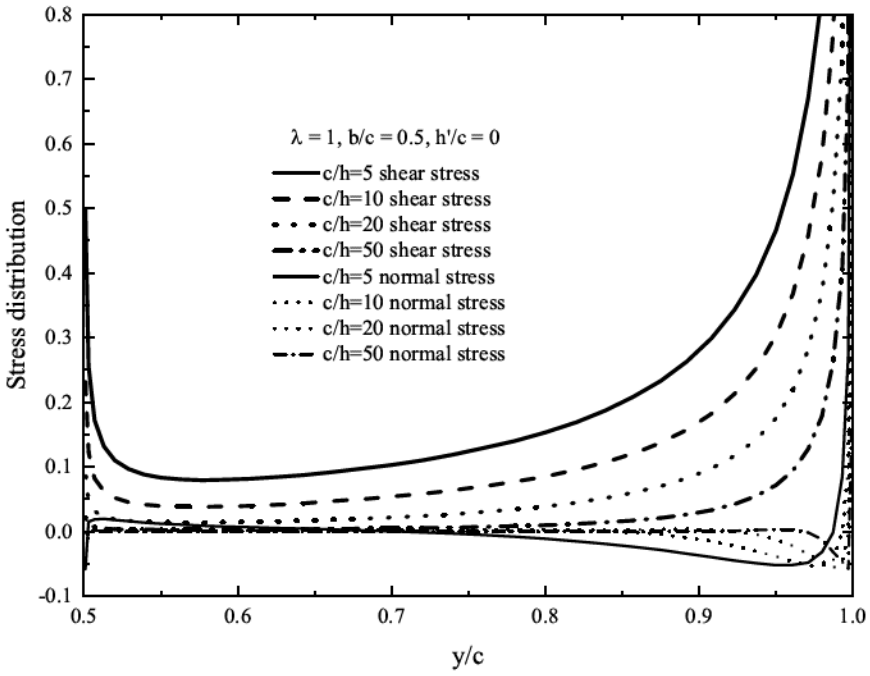

Figure 5.12: Shear stress distribution of current model for partial debonding actuators ($\lambda = 1$, $b/c = 0.5$ and $h^{'}/c = 0$).

softer (larger λ), the normalized axial displacement decreases. When λ is very large, the remaining actuator will act as a fixed boundary, limiting the axial displacement.

5.4 The case for the interacting of the two piezoelectric actuators

To evaluate the interaction between multiple actuators, two identical actuators bonded to an elastic host structure are investigated, as shown in figure 5.20. In this case $2b$ represents the distance between the two actuators. Five normalized distances $b/c = 0.7$, 0.5, 0.3, 0.1 and 0.01 are selected for $\lambda = 1$ and $c/h = 10$. Figures 5.21 and 5.22 show the normalized shear stress and normal stress distributions along the piezoelectric actuator with and without adhesively layer, respectively. $y/c = 1$ corresponds to the outer end of the actuator, $y/c = -1$ corresponds to its inner end of the actuator. The results are shown in figures 5.21

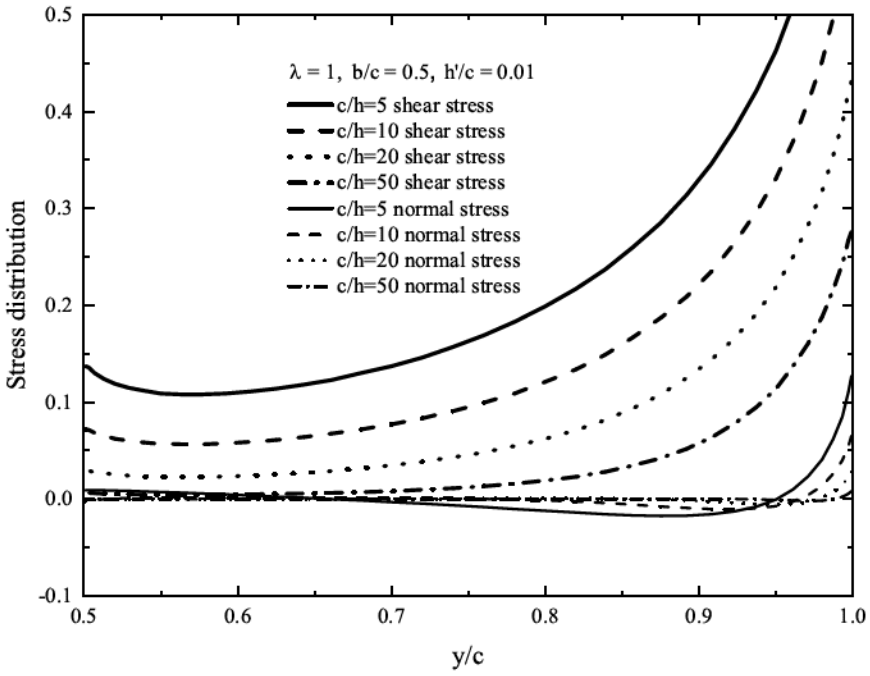

Figure 5.13: Normal stress distribution of current model for partial debonding actuators ($\lambda = 1$, $b/c = 0.5$ and $h^{'}/c = 0.01$).

and 5.22. It is observed that with the decrease of the distance, the stress magnitudes become unsymmetrical, which is induced by the interaction between the two bonded piezoelectric actuators. Although the stress near the inner end is significantly affected by the interaction, it is interesting to note that the stress at the outer end show very limited effect of the interaction. After considering the adhesive layer, the stress magnitudes become less unsymmetrical, especially for the normal stress. Also, the level of stress concentration at the ends of the piezoelectric actuators decrease.

5.5 Concluding remarks

This chapter is focused on the effects of material properties, the geometry and the adhesive layer on the load transfer between the piezoelectric actuator and the host structure. The

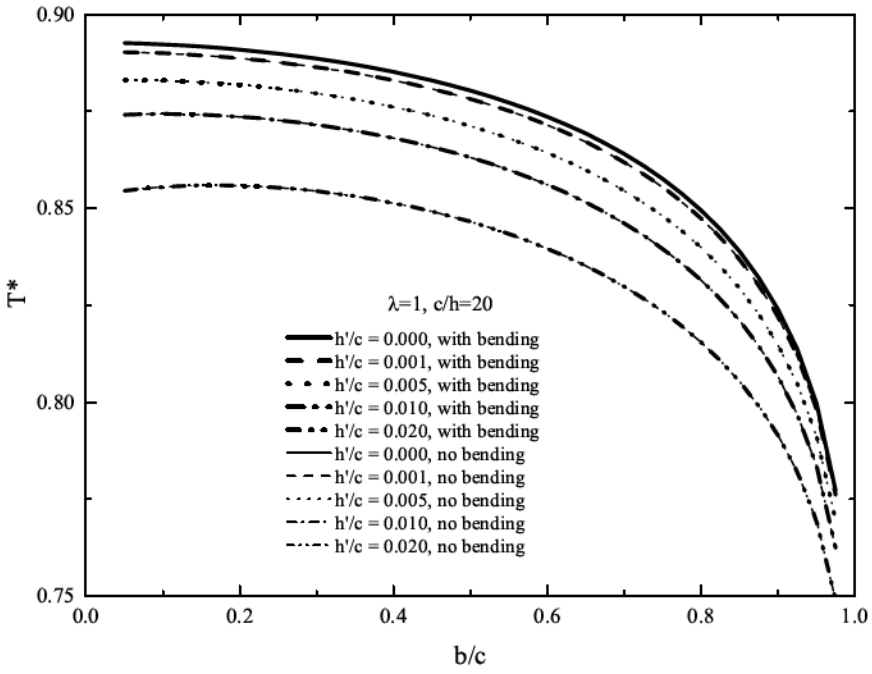

Figure 5.14: The normalized axial force of current model at the tips of the debonded part ($c/h = 20$ and $\lambda = 1$).

validity of the current model has been demonstrated by comparing with FEM results. The simulation results indicate that adhesive layer can reduce the stress concentration level at the ends of the piezoelectric actuator and increase the stress level along the piezoelectric actuator. Then, for actuator with partial debonding, the redistribution of the interfacial shear and normal stresses under different material and geometry conditions has been discussed. Similar to situation without debonding, the increase of the adhesive layer thickness can reduce stress concentration at the tips of debonded part and increase the stress level. The variation of the normalized bending moment, axial force and axial displacement with the normalized debonding length is also investigated for various adhesive layer thicknesses and material mismatches. The introduction of bending effect provides a more accurate description of the deformation and loading condition in the debonded part of the piezoelectric

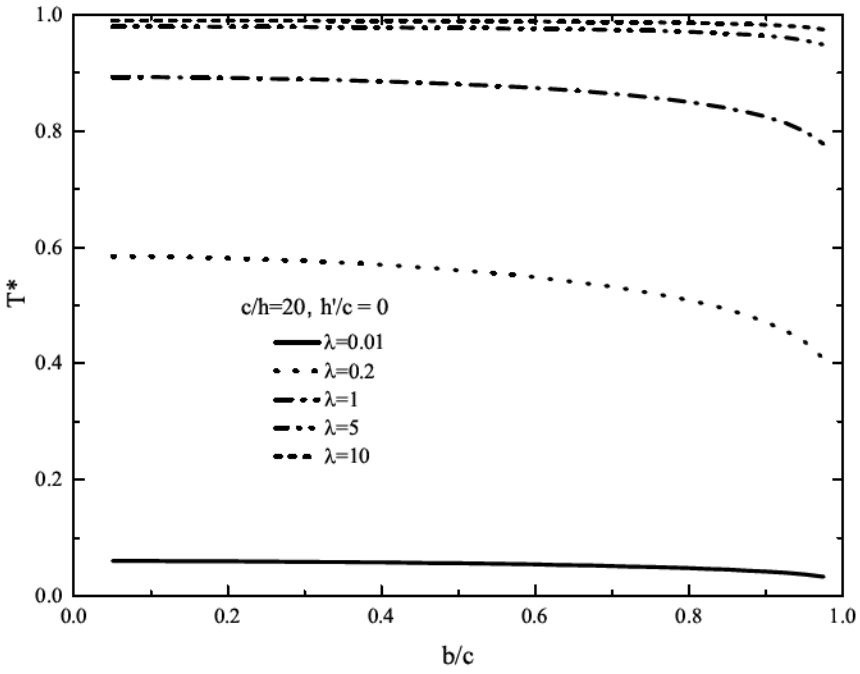

Figure 5.15: The normalized axial force of current model at the tips of the debonded part with different λ ($c/h = 20$ and $h'/c = 0.000$).

actuator, however, the axial force and displacement at the tips of debonded part keep almost the same after adding the bending effect. With the increase of the debonded length, the normalized bending moment and axial displacement increased. However, the normalized axial force decreases slightly when the debonding length increases. The interaction of two piezoelectric actuators has also been studied. With the decrease of the distance between the two bonding actuators, the magnitudes of the normal and shear stresses become unsymmetrical, corresponding to the direct interaction between the actuators. With the adhesive layer included the stress magnitudes become less unsymmetrical, especially for the normal stress, indicating relatively weaker interaction.

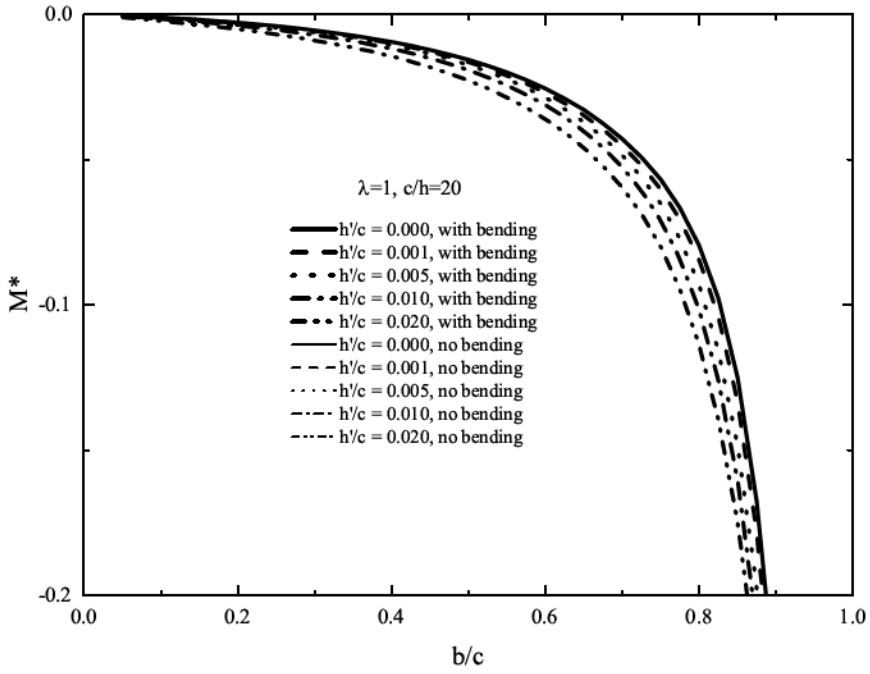

Figure 5.16: The normalized bending moment of current model at the tips of the debonded part ($\lambda = 1$ and $c/h = 20$).

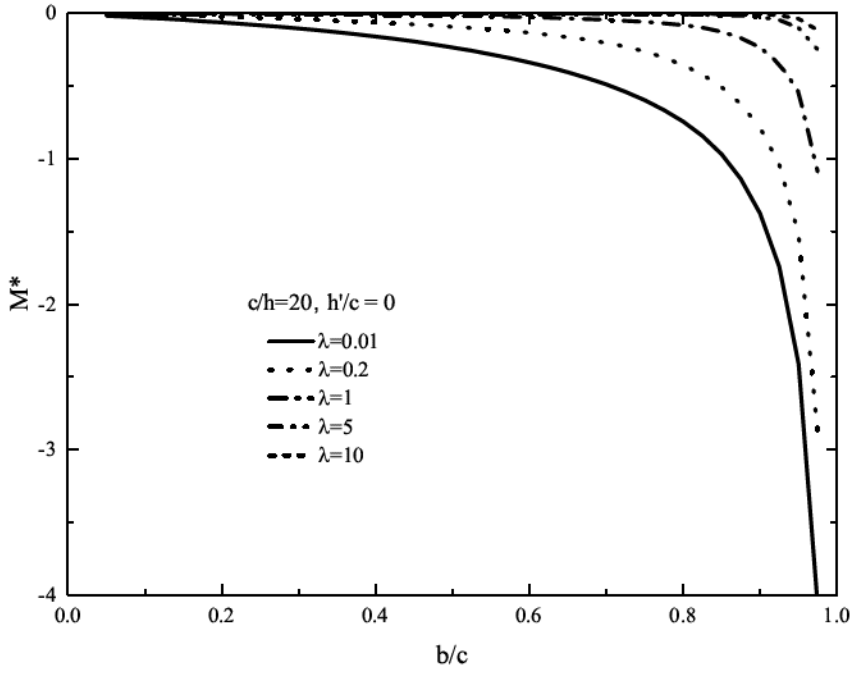

Figure 5.17: The normalized bending moment of current model at the tips of the debonded part with different λ ($c/h = 20$ and $h'/c = 0$).

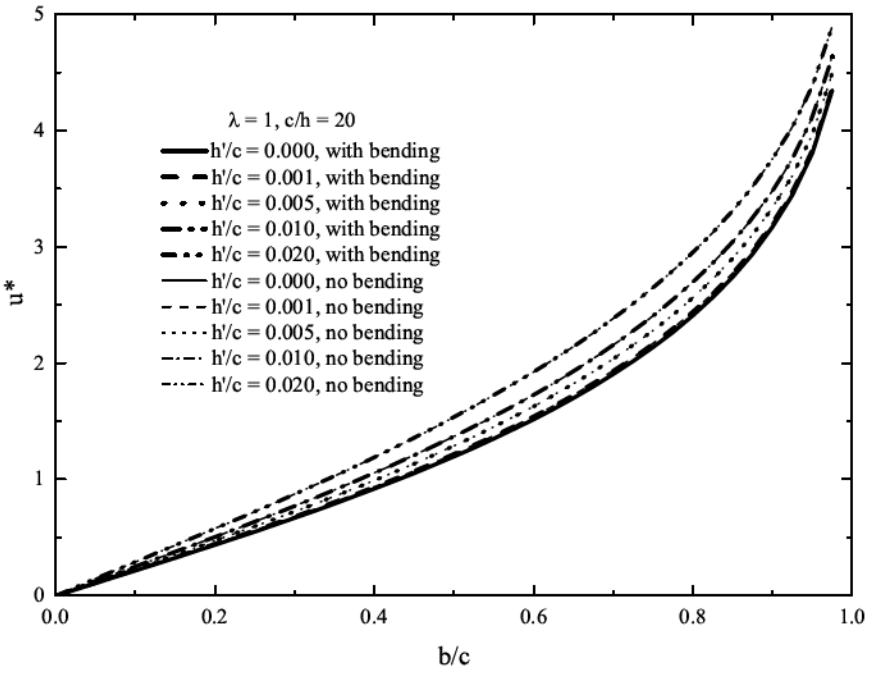

Figure 5.18: The normalized axial displacement of current model at the tips of the debonded part ($\lambda = 1$ and $c/h = 20$).

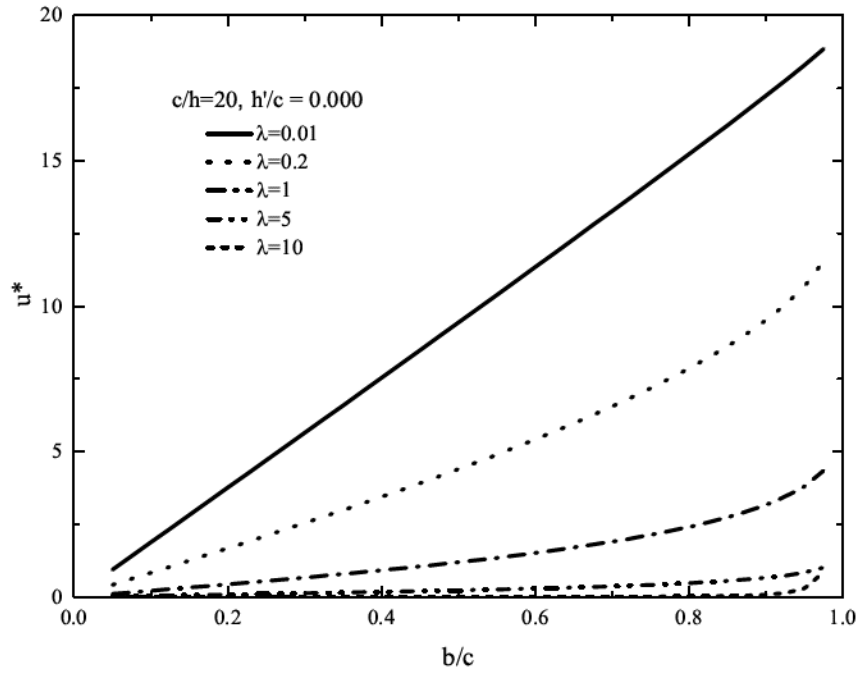

Figure 5.19: The normalized axial displacement of current model at the tips of the debonded part with different λ ($c/h = 20$ and $h'/c = 0$).

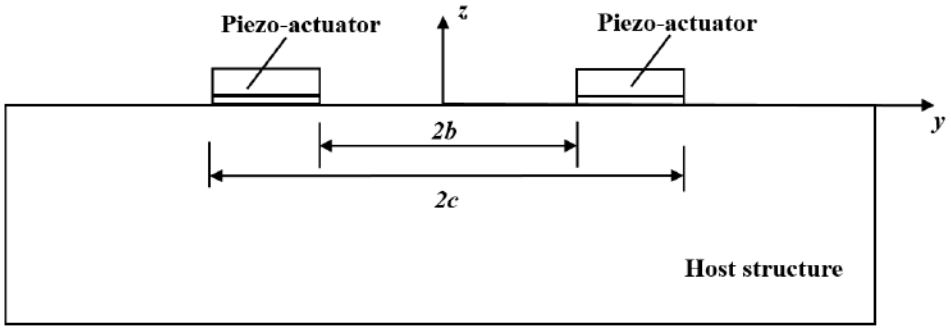

Figure 5.20: The schematic configuration of two piezoelectric actuators.

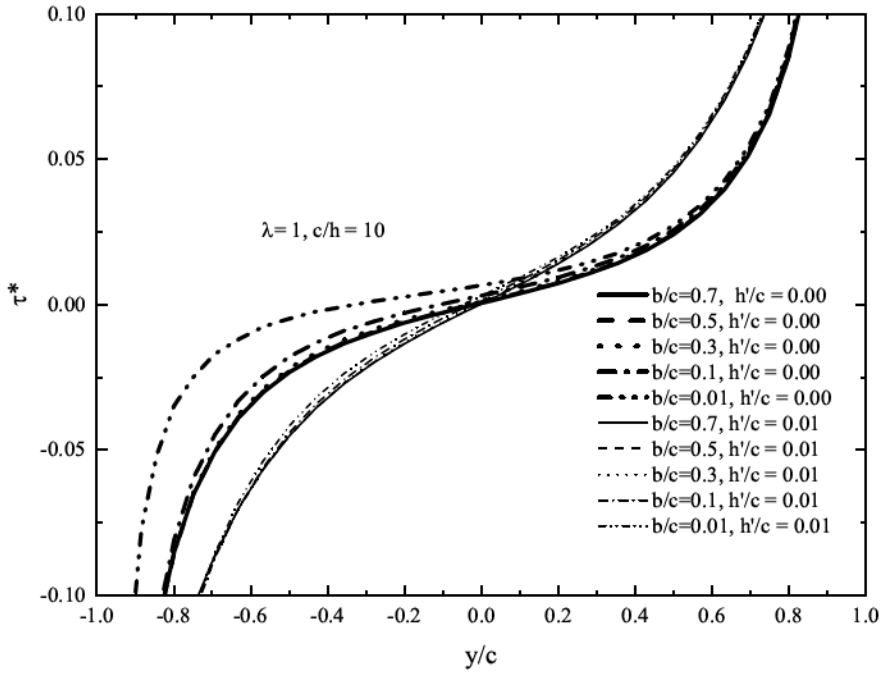

Figure 5.21: The normalized shear stress distribution of current model for interacting actuators ($\lambda = 1$ and $c/h = 10$).

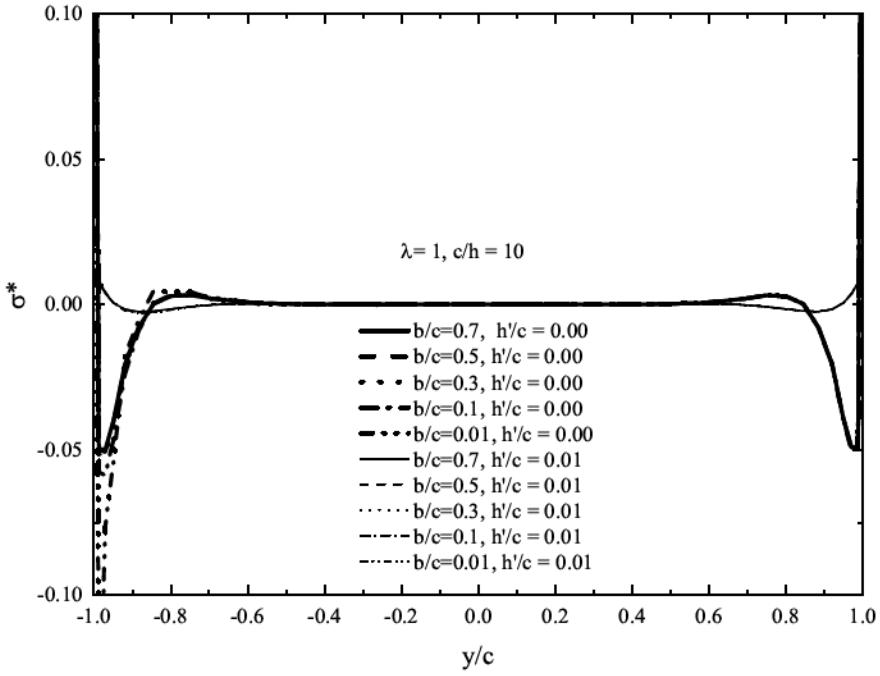

Figure 5.22: The normalized normal stress distribution of current model for interacting actuators ($\lambda = 1$ and $c/h = 10$).

Chapter 6: Contributions and future work

This chapter summarizes the main contributions of this thesis on the modelling of piezoelectric actuator and illustrates several problems that remain to be addressed in the subsequent research.

6.1 Main contributions and Conslusions

This thesis aims to estimate the effects of the imperfect bonding condition on the static electromechanical behavior of the surface-bonded piezoelectric actuators. This study is an extension of the previous work, in which an adhesive layer is included between a piezoelectric sensor/actuotor and an semi-infinite host structure and only the interfacial shear stress is considered (Jin and Wang, 2011a,b). The main contributions of this thesis to the field of the research are summarized as follows.

1. A new theoretical model considering the bending deformation of the thin-sheet piezoelectric actuator with an adhesive layer has been established. The integrated system contains an elastic semi-infinite host structure, attached by an adhesive layer and then a piezoelectric actuator on the top of adhesive layer under inplane electric loading.

2. The theoretical analysis and the corresponding FEM simulations have been conducted under static loading conditions. Considering that piezoelectric actuators are mostly used under dynamic loading conditions. The current model is corresponding to a quasi-static loading condition where the loading frequency is so low that the wavelength is much larger than the length of the piezoelectric actuator. The effects of the geometry, the material

mismatch, the material property of the piezoelectric actuator on the electromechanical behaviour of the system have been analyzed, for the cases under perfect bonding and partial debonding conditions.

3. The results of the study provide guidelines for the design of piezoelectric actuator systems. For example, with the existence of the adhesive layer, the stress concentration at the ends of actuator is decreased. The results also indicate that the thickness of the adhesive layer significantly affects the stress distribution. Thicker adhesive layers possess lower stress concentration around the ends of the piezoelectric actuators. Thus, there is less chance to peel off of the piezoelectric actuator from the host structure.

The specific conclusions, based on the results and observations on the variations of the interfacial stresses, the axial force, the bending moment and the axial displacement conducted in chapter 5, are as follows.

1. It is found that in order to reduce the interfacial stress concentration, the piezoelectric layer should be bonded to the host structure through an adhesive layer with low stiffness, namely large thickness.

2. The level of the interfacial stress concentration is closely related to the ratio of the length to thickness of the piezoelectric actuator. When the ratio decreases, the stress concentration will decrease. Also, larger thickness of the adhesive layer will make the model more resistant to the debonding between the piezoelectric actuator and the host structure.

3. The material combination of the piezoelectric actuator and the host structure needs to be carefully determined. When the piezoelectric material is very soft in comparison with the host structure, the bending moments at the two debonded tips approach zero and the

axial force is close to the blocking force of the piezoelectric actuator, corresponding to a high stress concentration near the ends of the piezoelectric actuator. A stiffer piezoelectric actuator will induce higher interfacial stress in the interior of the interface.

4. The debonding length also has a substantial influence on the interfacial stresses. With the increasing debonding length, the interfacial stress concentration level at the debonding tips becomes higher.

These conclusions could be potentially helpful for the design of smart systems and structures with piezoelectric actuators.

6.2 Future work

One of the main objectives of this thesis is to investigate the effect of the adhesive layer properties on the static electromechanical behaviour of the piezoelectric system with bending deformation. Although this thesis has tried to cover the important challenges and limitations of the current model with piezoelectric actuators, there are still some issues that need to be further addressed in the future work, which are listed as follow.

1. Under certain loading conditions, buckling of the debonding actuator may occur. The effect of the buckling of the piezoelectric actuator could be considered to better investigate the electromechanical behaviour of the system.

2. To make the piezoelectric model more realistic, it could be extended from two dimensions into three dimensions.

3. This thesis is mainly based on the theoretical analysis and FEM simulations of the piezoelectric model. The results of current model with bending match the FEM results very

well. However, corresponding experiments need to be conducted to validate the effectiveness of the current piezoelectric model. Proper modification of the model may be needed according to experiment results.

4. Some cracks with different sizes and orientations could be introduced into the host medium to form a health monitoring system, which could show the potentials of this model for practical applications.

Bibliography

Akella, P., Chen, X., Cheng, W., Hughes, D., and Wen, J. T. Modeling and control of smart structures with bonded piezoelectric sensors and actuators. *Smart Materials and Structures*, 3(3):344–353, 1994.

Alleyne, D. N. and Cawley, P. Optimization of lamb wave inspection techniques. *NDT E International*, 25(1):11–22, 1992.

Allik, H. and Hughes, T. J. Finite element method for piezoelectric vibration. *International journal for numerical methods in engineering*, 2(2):151–157, 1970.

Annamdas, V. G. M. and Soh, C. K. Application of electromechanical impedance technique for engineering structures: Review and future issues. *Journal of Intelligent Material Systems and Structures*, 21(1):41–59, 2010.

Bailey, T. and Hubbard, J. E. Distributed piezoelectric-polymer active vibration control of a cantilever beam. *Journal of Guidance, Control, and Dynamics*, 8(5):605–611, 1985.

Benjeddou, A. Advances in piezoelectric finite element modeling of adaptive structural elements: a survey. 76(1):347–363, 2000.

Bhalla, S. and Bajaj, S. Bone characterization using piezotransducers as biomedical sensors. *Strain*, 44(6):475–478, 2008.

Boemio, G., Rizzo, P., and Nardo, L. D. Assessment of dental implant stability by means of the electromechanical impedance method. *Smart Materials and Structures*, 20(4): 045008, 2011.

Boller, C. Next generation structural health monitoring and its integration into aircraft design. *International Journal of Systems Science*, 31(11):1333–1349, 2000.

Bourasseau, N., Moulin, E., Delebarre, C., and Bonniau, P. Radome health monitoring with lamb waves: experimental approach. *NDT E International*, 33(6):393–400, 2000.

Calio, R., Rongala, U. B., Camboni, D., Milazzo, M., Stefanini, C., De Petris, G., and Oddo, C. M. Piezoelectric energy harvesting solutions. *Sensors*, 14(3):4755–4790, 2014.

Chen, P., Chen, S., Guo, W., and Gao, F. The interface behavior of a thin piezoelectric film bonded to a graded substrate. *Mechanics of Materials*, 127:26–38, 2018a.

Chen, P., Peng, J., Liu, H., Gao, F., and Guo, W. The electromechanical behavior of a piezoelectric actuator bonded to a graded substrate including an adhesive layer. *Mechanics of Materials*, 123:77–87, 2018b.

Choi, S.-B. and Han, Y.-M. *Piezoelectric actuators: control applications of smart materials*. CRC Press, 2016. ISBN 1439818096.

Crawley, E. F. and Anderson, E. H. Detailed models of piezoceramic actuation of beams. *Journal of Intelligent Material Systems and Structures*, 1(1):4–25, 1990.

Crawley, E. F. and De Luis, J. Use of piezoelectric actuators as elements of intelligent structures. *AIAA journal*, 25(10):1373–1385, 1987.

Della, C. N. and Shu, D. Vibration of delaminated composite laminates: A review. *Applied Mechanics Reviews*, 60(1):1–20, 2007.

Denoyer, K. K. and Kwak, M. K. Dynamic modelling and vibration suppression of a swelling structure utilizing piezoelectric sensors and actuators. *Journal of Sound and Vibration*, 189(1):13–31, 1996.

Dimitriadis, E. K., Fuller, C. R., and Rogers, C. A. Piezoelectric actuators for distributed vibration excitation of thin plates. *Journal of Vibration and Acoustics*, 113(1):100–107, 1991.

Duan, W. H., Wang, Q., and Quek, S. T. Applications of piezoelectric materials in structural health monitoring and repair: Selected research examples. *Materials (Basel)*, 3(12): 5169–5194, 2010.

Faria, A. R. d. The impact of finite-stiffness bonding on the sensing effectiveness of piezoelectric patches. *Smart Materials and Structures*, 12(4):N5–N8, 2003.

Garg, A. C. Delamination - a damage mode in composite structures. *Engineering Fracture Mechanics*, 29(5):557–584, 1988.

Ghosh, T., Kundu, T., and Karpur, P. Efficient use of lamb modes for detecting defects in large plates. *Ultrasonics*, 36(7):791–801, 1998.

Giurgiutiu, V. *Structural health monitoring: with piezoelectric wafer active sensors*. Elsevier, 2007. ISBN 0080556795.

Giurgiutiu, V. and Zagrai, A. Damage detection in thin plates and aerospace structures with the electro-mechanical impedance method. *Structural Health Monitoring*, 4(2):99–118, 2005.

Giurgiutiu, V., Zagrai, A., and Jing Bao, J. Piezoelectric wafer embedded active sensors for aging aircraft structural health monitoring. *Structural Health Monitoring*, 1(1):41–61, 2002.

Giurgiutiu, V., Zagrai, A., and Bao, J. Damage identification in aging aircraft structures with piezoelectric wafer active sensors. *Journal of Intelligent Material Systems and Structures*, 15(9-10):673–687, 2004.

Glushkov, E., Glushkova, N., Kvasha, O., and Seemann, W. Integral equation based modeling of the interaction between piezoelectric patch actuators and an elastic substrate. *Smart Materials and Structures*, 16(3):650–664, 2007.

Gu, H., Song, G., Dhonde, H., Mo, Y. L., and Yan, S. Concrete early-age strength monitoring using embedded piezoelectric transducers. *Smart Materials and Structures*, 15(6): 1837–1845, 2006.

Ha, S. K., Keilers, C., and Chang, F.-K. Finite element analysis of composite structures containing distributed piezoceramic sensors and actuators. *AIAA journal*, 30(3):772–780, 1992.

Han, L., Wang, X. D., and Sun, Y. The effect of bonding layer properties on the dynamic behaviour of surface-bonded piezoelectric sensors. *International Journal of Solids and Structures*, 45(21):5599–5612, 2008a.

Han, L., Wang, X. D., and Zuo, M. The dynamic behavior of a surface-bonded piezoelectric actuator with a bonding layer. *Acta Mechanica*, 206(3):193, 2008b.

Huang, B., Kim, H. S., and Yoon, G. H. Modeling of a partially debonded piezoelectric actuator in smart composite laminates. *Smart Materials and Structures*, 24(7):075013, 2015.

Huang, G., Song, F., and Wang, X. Quantitative modeling of coupled piezo-elastodynamic behavior of piezoelectric actuators bonded to an elastic medium for structural health monitoring: a review. *Sensors (Basel)*, 10(4):3681–702, 2010.

Hwang, W.-S. and Park, H. C. Finite element modeling of piezoelectric sensors and actuators. *AIAA journal*, 31(5):930–937, 1993.

Ihn, J.-B. and Chang, F.-K. Detection and monitoring of hidden fatigue crack growth using a built-in piezoelectric sensor/actuator network: I. diagnostics. *Smart Materials and Structures*, 13(3):609–620, 2004.

Im, S. and N. Atluri, S. *Effects of a piezo-actuator on a finitely deformed beam subjected togeneral loading*, volume 27. 1989.

Jaffe, B. *Piezoelectric Ceramics*. Elsevier Science, 2012.

Jin, C. and Wang, X. The effect of adhesive layers on the dynamic behavior of surface-bonded piezoelectric sensors with debonding. *Journal of Intelligent Material Systems and Structures*, 22(7):655–670, 2011a.

Jin, C. and Wang, X. Analytical modelling of the electromechanical behaviour of surface-bonded piezoelectric actuators including the adhesive layer. *Engineering Fracture Mechanics*, 78(13):2547–2562, 2011b.

K Chai, W. and Arnold, S. *Structronics and Actuation of Hybrid Electrostrictive/ Piezoelectric Thin Shells*, volume 128. 2006.

Kim, H. S., Kim, J.-H., and Kim, J. A review of piezoelectric energy harvesting based on vibration. *International journal of precision engineering and manufacturing*, 12(6): 1129–1141, 2011.

Kusculuoglu, Z. K., Fallahi, B., and Royston, T. J. *New constitutive model for vibrations of a beam with a piezoceramic patch actuator*, volume 4693 of *SPIE's 9th Annual International Symposium on Smart Structures and Materials*. SPIE, 2002.

Kwak, M. K. and Sciulli, D. Fuzzy-logic based vibration suppression control experiments on active structures. *Journal of Sound and Vibration*, 191(1):15–28, 1996.

Levi, D. S., Kusnezov, N., and Carman, G. P. Smart materials applications for pediatric cardiovascular devices. *Pediatric Research*, 63:552, 2008.

Li, Z. and Wang, X. On the dynamic behaviour of a two-dimensional elastic metamaterial system. *International Journal of Solids and Structures*, 78-79:174–181, 2016.

Li, Z., Hu, H., and Wang, X. A new two-dimensional elastic metamaterial system with multiple local resonances. *International Journal of Mechanical Sciences*, 149:273–284, 2018.

Li, Z., Wang, C., and Wang, X. Modelling of elastic metamaterials with negative mass and modulus based on translational resonance. *International Journal of Solids and Structures*, 162:271–284, 2019.

Liang, C., Sun, F., and Rogers, C. Coupled electro-mechanical analysis of adaptive material systems - determination of the actuator power consumption and system energy transfer. *Journal of Intelligent Material Systems and Structures*, 5(1):12–20, 1994.

Liang, W., Rui-xiang, B., and Cheng, Y. Interfacial debonding behavior of composite beam/plates with pzt patch. *Composite Structures*, 92(6):1410–1415, 2010.

Lim, Y. Y., Kwong, K. Z., Liew, W. Y. H., and Soh, C. K. Non-destructive concrete strength evaluation using smart piezoelectric transducer - a comparative study. *Smart Materials and Structures*, 25(8):085021, 2016.

Lim, Y. Y., Smith, S. T., and Soh, C. K. Wave propagation based monitoring of concrete curing using piezoelectric materials: Review and path forward. 99:50–63, 2018.

Liyong, T., Dongchang, S., and Satya, N. A. Sensing and actuating behaviours of piezoelectric layers with debonding in smart beams. *Smart Materials and Structures*, 10(4): 713, 2001a.

Liyong, T., Dongchang, S., and Satya, N. A. Sensing and actuating behaviours of piezoelectric layers with debonding in smart beams. *Smart Materials and Structures*, 10(4): 713, 2001b.

Lu, Y., Li, J., Ye, L., and Wang, D. Guided waves for damage detection in rebar-reinforced concrete beams. *Construction and Building Materials*, 47:370–378, 2013.

Luo, Q. and Tong, L. Exact static solutions to piezoelectric smart beams including peel stresses: I: Theoretical formulation. *International Journal of Solids and Structures*, 39 (18):4677–4695, 2002a.

Luo, Q. and Tong, L. Exact static solutions to piezoelectric smart beams including peel stresses. ii. numerical results, comparison and discussion. *International Journal of Solids and Structures*, 39(18):4697–4722, 2002b.

Mei, H., Haider, M. F., Joseph, R., Migot, A., and Giurgiutiu, V. Recent advances in piezoelectric wafer active sensors for structural health monitoring applications. *Sensors (Basel, Switzerland)*, 19(2):383, 2019.

Miller, S. E. and Abramovich, H. A self-sensing piezolaminated actuator model for shells using a first order shear deformation theory. *Journal of Intelligent Material Systems and Structures*, 6(5):624–638, 1995.

Milsom, R. F., Reilly, N. H. C., and Redwood, M. Analysis of generation and detection of surface and bulk acoustic waves by interdigital transducers. *IEEE Transactions on Sonics and Ultrasonics*, 24(3):147–166, 1977.

Mindlin, R. D. Forced thickness-shear and flexural vibrations of piezoelectric crystal plates. *Journal of Applied Physics*, 23(1):83–88, 1952.

Mindlin, R. High frequency vibrations of piezoelectric crystal plates. *International Journal of Solids and Structures*, 8(7):895–906, 1972.

Mitchell, J. and Reddy, J. A study of embedded piezoelectric layers in composite cylinders. *Journal of applied mechanics*, 62(1):166–173, 1995.

Monkhouse, R. S. C., Wilcox, P. W., Lowe, M. J. S., Dalton, R. P., and Cawley, P. The rapid monitoring of structures using interdigital lamb wave transducers. *Smart Materials and Structures*, 9(3):304–309, 2000.

Moulin, E., Assaad, J., Delebarre, C., and Osmont, D. Modeling of lamb waves generated by integrated transducers in composite plates using a coupled finite element-normal modes expansion method. *The Journal of the Acoustical Society of America*, 107(1): 87–94, 2000.

Muskhelishvili, N. *Some basic problems of the mathematical theory of elasticity*. Noordhoff: Groningen, 3rd edition, 1953.

Na, W. S. and Baek, J. A review of the piezoelectric electromechanical impedance based structural health monitoring technique for engineering structures. *Sensors*, 18(5):1307, 2018a.

Na, W. S. and Baek, J. A review of the piezoelectric electromechanical impedance based structural health monitoring technique for engineering structures. *Sensors*, 18(5):1307, 2018b.

Nakra, B. C. Vibration control in machines and structures using viscoelastic damping. *Journal of Sound and Vibration*, 211(3):449–466, 1998.

Newnham, R. E. and Ruschau, G. R. Electromechanical properties of smart materials. *Journal of Intelligent Material Systems and Structures*, 4(3):289–294, 1993.

Otsuka, K. and Wayman, C. M. *Shape memory materials*. Cambridge university press, 1999. ISBN 0521663849.

Park, G., Cudney, H. H., and Inman, D. J. Impedance-based health monitoring of civil structural components. *Journal of Infrastructure Systems*, 6(4):153–160, 2000a.

Park, G., Sohn, H., Farrar, C. R., and Inman, D. J. Overview of piezoelectric impedance-based health monitoring and path forward. *Shock and Vibration Digest*, 35(6):451–464, 2003.

Park, J.-M., Kim, D.-S., and Han, S.-B. Properties of interfacial adhesion for vibration controllability of composite materials as smart structures. *Composites Science and Technology*, 60(10):1953–1963, 2000b.

Park, J.-M., Kim, D.-S., and Han, S.-B. Properties of interfacial adhesion for vibration controllability of composite materials as smart structures. *Composites Science and Technology*, 60(10):1953–1963, 2000c.

Pietrzakowski, M. Active damping of beams by piezoelectric system: effects of bonding layer properties. *International Journal of Solids and Structures*, 38(44):7885–7897, 2001.

Prakah-Asante, K. O. and Craig, K. C. The application of multi-channel design methods for vibration control of an active structure. *Smart Materials and Structures*, 3(3):329–343, 1994.

Qing, X., Li, W., Wang, Y., and Sun, H. Piezoelectric transducer-based structural health monitoring for aircraft applications. *Sensors (Basel, Switzerland)*, 19(3):545, 2019.

Rabinovitch, O. and Vinson, J. R. Adhesive layer effects in surface-mounted piezoelectric actuators. *Journal of Intelligent Material Systems and Structures*, 13(11):689–704, 2002a.

Rabinovitch, O. and Vinson, J. R. Adhesive layer effects in surface-mounted piezoelectric actuators. *Journal of Intelligent Material Systems and Structures*, 13(11):689–704, 2002b.

Rahmoune, M., Benjeddou, A., Ohayon, R., and Osmont, D. New thin piezoelectric plate models. *Journal of intelligent material systems and structures*, 9(12):1017–1029, 1998.

Reddy, J. N. On laminated composite plates with integrated sensors and actuators. *Engineering Structures*, 21(7):568–593, 1999.

Ribolla, E. L. M. and Rizzo, P. Modelling the electromechanical impedance method for the prediction of the biomechanical behavior of dental implant stability. *Procedia Engineering*, 109:128–134, 2015.

Schwartz, M. M. *Smart materials*. CRC Press, Boca Raton, 2009. ISBN 9781420043730 1420043730 1281892181 9781281892188.

Seeley, C. and Chattopadhyay, A. Modeling delaminations in smart composite laminates. In *Adaptive Structures Forum*, page 1276, 1996.

Shen, N. H. Analysis of beams containing piezoelectric sensors and actuators. *Smart Materials and Structures*, 3(4):439–447, 1994.

Soh, C., Tseng, K. K., Bhalla, S., and Gupta, A. Performance of smart piezoceramic patches in health monitoring of a rc bridge. *Smart materials and Structures*, 9(4):533, 2000.

Song, F., Huang, G. L., Kim, J. H., and Haran, S. On the study of surface wave propagation in concrete structures using a piezoelectric actuator/sensor system. *Smart Materials and Structures*, 17(5):055024, 2008.

Staszewski, W. J., Mahzan, S., and Traynor, R. Health monitoring of aerospace composite structures - active and passive approach. *Composites Science and Technology*, 69(11): 1678–1685, 2009.

Sun, D., Tong, L., and Atluri, S. N. Effects of piezoelectric sensor/actuator debonding on vibration control of smart beams. *International Journal of Solids and Structures*, 38(50): 9033–9051, 2001.

Sun, F. P., Chaudhry, Z., Liang, C., and Rogers, C. A. Truss structure integrity identification using pzt sensor-actuator. *Journal of Intelligent Material Systems and Structures*, 6(1): 134–139, 1995.

Tan, K. S., Guo, N., Wong, B. S., and Tui, C. G. Comparison of lamb waves and pulse echo in detection of near-surface defects in laminate plates. 28(4):215–223, 1995.

Tani, J., Takagi, T., and Qiu, J. Intelligent material systems: Application of functional materials. *Applied Mechanics Reviews*, 51(8):505–521, 1998.

Tawie, R. and Lee, H. K. Characterization of cement-based materials using a reusable piezoelectric impedance-based sensor. *Smart Materials and Structures*, 20(8):085023, 2011.

Tua, P. S., Quek, S. T., and Wang, Q. Detection of cracks in plates using piezo-actuated lamb waves. *Smart Materials and Structures*, 13(4):643–660, 2004.

Tua, P. S., Quek, S. T., and Wang, Q. Detection of cracks in cylindrical pipes and plates using piezo-actuated lamb waves. *Smart Materials and Structures*, 14(6):1325–1342, 2005.

Tylikowski, A. Effects of piezoactuator delamination on the transfer functions of vibration control systems. *International Journal of Solids and Structures*, 38(10):2189–2202, 2001a.

Tylikowski, A. Effects of piezoactuator delamination on the transfer functions of vibration control systems. *International Journal of Solids and Structures*, 38(10):2189–2202, 2001b.

Tzou, H. S. and Gadre, M. Theoretical analysis of a multi-layered thin shell coupled with piezoelectric shell actuators for distributed vibration controls. *Journal of Sound and Vibration*, 132(3):433–450, 1989.

Tzou, H. S. and Tseng, C. I. Distributed piezoelectric sensor/actuator design for dynamic measurement/control of distributed parameter systems: A piezoelectric finite element approach. *Journal of Sound and Vibration*, 138(1):17–34, 1990.

Tzou, H. S., Bao, Y., and Venkayya, V. B. Parametric study of segmented transducers laminated on cylindrical shells, part 2: Actuator patches. *Journal of Sound and Vibration*, 197(2):225–249, 1996.

Tzou, H. S., Wang, D. W., and Chai, W. K. Dynamics and distributed control of conical shells laminated with full and diagonal actuators. *Journal of Sound and Vibration*, 256 (1):65–79, 2002.

Wang, B. L. and Mai, Y. W. Fracture of a piezoelectric material layer bonded by two elastic layers. *International Journal of Engineering Science*, 40(15):1697–1727, 2002.

Wang, C. S. and Chang, F. K. *Built-in diagnostics for impact damage identification of composite structures.* 1999.

Wang, L., Bai, R.-x., and Chen, H. Analytical modeling of the interface crack between a piezoelectric actuator and an elastic substrate considering shear effects. *International Journal of Mechanical Sciences*, 66:141–148, 2013.

Wang, S. Y., Quek, S. T., and Ang, K. K. Vibration control of smart piezoelectric composite plates. *Smart Materials and Structures*, 10(4):637–644, 2001.

Wang, X. D. and Meguid, S. A. On the electroelastic behaviour of a thin piezoelectric actuator attached to an infinite host structure. *International Journal of Solids and Structures*, 37(23):3231–3251, 2000.

Wang, X. Dynamic behaviour of a metamaterial system with negative mass and modulus. *International Journal of Solids and Structures*, 51(7):1534–1541, 2014.

Xu, C. H., Zhou, Z. H., Xu, X. S., and Leung, A. Y. T. Electroelastic singularities and intensity factors for an interface crack in piezoelectric-elastic bimaterials. *Applied Mathematical Modelling*, 39(9):2721–2739, 2015.

Yang, J. *An Introduction to the Theory of Piezoelectricity*. Springer US, 2006.

Yang, Y., Lim, Y. Y., and Soh, C. K. Practical issues related to the application of the electromechanical impedance technique in the structural health monitoring of civil structures: I. experiment. *Smart Materials and Structures*, 17(3):035008, 2008.

Yousefsani, S. A. and Tahani, M. Edge effects in adhesively bonded composite joints integrated with piezoelectric patches. *Composite Structures*, 200:187–194, 2018.

Yousefsani, S. A. and Tahani, M. Analytical solutions for adhesively bonded composite single-lap joints under mechanical loadings using full layerwise theory. *International Journal of Adhesion and Adhesives*, 43:32–41, 2013.

Yu, H. and Wang, X. Modelling and simulation of surface-bonded piezoelectric actuators with bending effects. *Journal of Intelligent Material Systems and Structures*, 28(4):507–520, 2016.

Yu, L. and Giurgiutiu, V. In situ 2-d piezoelectric wafer active sensors arrays for guided wave damage detection. *Ultrasonics*, 48(2):117–134, 2008.

Zagrai, A., Doyle, D., Gigineishvili, V., Brown, J., Gardenier, H., and Arritt, B. Piezoelectric wafer active sensor structural health monitoring of space structures. *Journal of Intelligent Material Systems and Structures*, 21(9):921–940, 2010.

Zhang, S.-Q., Zhao, G.-Z., Rao, M. N., Schmidt, R., and Yu, Y.-J. A review on modeling techniques of piezoelectric integrated plates and shells. *Journal of Intelligent Material Systems and Structures*, 30(8):1133–1147, 2019.

Appendix

A.1 Effective material constants

This part is intended to provide the fundamental equations, which can fully describe the mechanical and electric properties of the piezoelectric materials. The general equation of motion is

$$\sigma_{ij,i} + f_i = \rho \ddot{u}_j. \tag{A1}$$

According to Gauss' law,

$$D_{i,i} = 0. \tag{A2}$$

The constitutive equations of the piezoelectric actuator are

$$\{\sigma\} = [c]\{\varepsilon\} - [e]\{E\}, \quad \{D\} = [e]\{\varepsilon\} + [\lambda]\{E\}, \tag{A3}$$

with the strain field $\{\varepsilon\}$ and the electric field intensity $\{E\}$ given by

$$\varepsilon_{ij} = \frac{1}{2}(u_{i,j} + u_{j,i}), \quad E_k = -V_{,k}. \tag{A4}$$

Here, $\{\sigma\}$ and $\{\varepsilon\}$ are the stress and strain fields, f_i and ρ represent the body force and the mass density, respectively. $\{D\}$, $\{E\}$ and V are the electric displacement, the electrical field and the potential, respectively. $[c]$ is elastic stiffness constant matrix for a constant electric potential, $[e]$ represents a tensor containing the piezoelectric constants and $[\lambda]$ represents

the dielectric constants for zero strains. Equation A3 can be rewritten in a matrix form as

$$\begin{bmatrix} \sigma_x \\ \sigma_y \\ \sigma_z \\ \sigma_{xz} \\ \sigma_{yz} \\ \sigma_{xy} \end{bmatrix} = \begin{bmatrix} c_{11} & c_{12} & c_{13} & 0 & 0 & 0 \\ c_{12} & c_{11} & c_{13} & 0 & 0 & 0 \\ c_{13} & c_{13} & c_{33} & 0 & 0 & 0 \\ 0 & 0 & 0 & c_{44} & 0 & 0 \\ 0 & 0 & 0 & 0 & c_{44} & 0 \\ 0 & 0 & 0 & 0 & 0 & c_{66} \end{bmatrix} \begin{bmatrix} \varepsilon_x \\ \varepsilon_y \\ \varepsilon_z \\ 2\varepsilon_{xz} \\ 2\varepsilon_{yz} \\ 2\varepsilon_{xy} \end{bmatrix} - \begin{bmatrix} 0 & 0 & e_{31} \\ 0 & 0 & e_{31} \\ 0 & 0 & e_{33} \\ 0 & e_{15} & 0 \\ e_{15} & 0 & 0 \\ 0 & 0 & 0 \end{bmatrix} \begin{bmatrix} E_x \\ E_y \\ E_z \end{bmatrix}, \tag{A5}$$

$$\begin{bmatrix} D_x \\ D_y \\ D_z \end{bmatrix} = \begin{bmatrix} 0 & 0 & 0 & 0 & e_{15} & 0 \\ 0 & 0 & 0 & e_{15} & 0 & 0 \\ e_{31} & e_{31} & e_{33} & 0 & 0 & 0 \end{bmatrix} \begin{bmatrix} \varepsilon_x \\ \varepsilon_y \\ \varepsilon_z \\ 2\varepsilon_{xz} \\ 2\varepsilon_{yz} \\ 2\varepsilon_{xy} \end{bmatrix} + \begin{bmatrix} \lambda_{11} & 0 & 0 \\ 0 & \lambda_{11} & 0 \\ 0 & 0 & \lambda_{33} \end{bmatrix} \begin{bmatrix} E_x \\ E_y \\ E_z \end{bmatrix}. \tag{A6}$$

In this study, plane strain condition is assumed, which means $\varepsilon_x = 0$. Then, the following relation can be obtained from equation (A4)

$$\sigma_y = c_{11}\varepsilon_y + c_{13}\varepsilon_z - e_{31}E_z, \tag{A7}$$

$$\sigma_z = c_{13}\varepsilon_y + c_{33}\varepsilon_z - e_{33}E_z, \tag{A8}$$

$$D_z = e_{31}\varepsilon_y + e_{33}\varepsilon_z + \lambda_{33}E_z. \tag{A9}$$

Equations (A7) and (A9) also can be rearranged as

$$\sigma_y = E^* \varepsilon_y - e_{31}^* E_z, \tag{A10}$$

$$D_z = e_{31}^* \varepsilon_y + \lambda_{33}^* E_z, \tag{A11}$$

in which E^*, e_{31}^*, and λ_{33}^* are the effective material constants of the piezoelectric actuator model. According to the electroelastic line actuator model, these material constants are given by

$$E^* = c_{11} - \frac{c_{13}^2}{c_{33}}, \quad e_{31}^* = e_{31} - e_{33}\frac{c_{13}}{c_{33}}, \quad \lambda_{33}^* = \frac{e_{33}^2}{c_{33}} + \lambda_{33}, \tag{A12}$$

where the poling direction is designated along the z-axis.

A.2 The properties used in the context of Chebyshev polynomials

The polynomial of the first kind $T_i(x)$ is defined as

$$T_i(x) = \cos(i \arccos x), \tag{A13}$$

or equivalently

$$T_i(\cos\theta) = \cos(i\theta). \tag{A14}$$

The polynomial of the second kind $U_i(x)$ is defined as

$$U_i(x) = \sin(i \arcsin x), \tag{A15}$$

or equivalently

$$U_i(\cos\theta) = \frac{\sin(i+1)\theta}{\sin\theta}. \tag{A16}$$

In what follows, the following relation can be obtained

$$T_i'(x) = iU_{i-1}(x). \tag{A17}$$

A direct integration of the Chebyshev polynomial of first kind $T_i(x)$ on the interval $[-1,1]$ can be derived,

$$\int_{-1}^{1} \frac{T_i(x)}{(x-y)\sqrt{(1-x^2)}} dx = \pi U_{i-1}(y), \quad i > 1 \ \ and \ \ |y| < 1. \tag{A18}$$

The polynomials of the first kind $T_i(x)$ are orthogonal with respect to the weight function $\frac{1}{\sqrt{(1-x^2)}}$ on the interval $[-1,1]$,

$$\frac{1}{\pi}\int_{-1}^{1} \frac{T_i(x)T_j(x)}{\sqrt{(1-x^2)}} dx = \begin{cases} 0, & i \neq j, \\ 1, & i = j = 0, \\ 1/2, & i = j \geq 1. \end{cases} \tag{A19}$$